

Saliency-Guided Training for Fingerprint Presentation Attack Detection

Samuel Webster

Adam Czajka

Department of Computer Science and Engineering
University of Notre Dame, IN, USA

{swebster, aczajka}@nd.edu

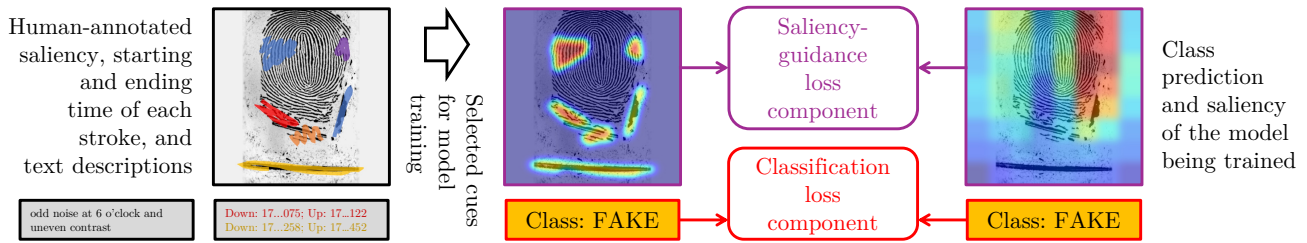


Figure 1. We collected visual salient annotations and text descriptions, supporting decisions of humans detecting fake fingerprints, and used these salient features in saliency-guided model training paradigm to offer an effective fingerprint presentation attack detection method.

Abstract

Saliency-guided training, which directs model learning to important regions of images, has demonstrated generalization improvements across various biometric presentation attack detection (PAD) tasks. This paper presents its first application to fingerprint PAD. We conducted a 50-participant study to create a dataset of 800 human-annotated fingerprint perceptually-important maps, explored alongside algorithmically-generated ‘‘pseudosalient,’’ including minutiae-based, image quality-based, and autoencoder-based saliency maps. Evaluating on the 2021 Fingerprint Liveness Detection Competition testing set, we explore various configurations within five distinct training scenarios to assess the impact of saliency-guided training on accuracy and generalization. Our findings demonstrate the effectiveness of saliency-guided training for fingerprint PAD in both limited and large data contexts, and we present a configuration capable of earning the first place on the LivDet-2021 benchmark. Our results highlight saliency-guided training’s promise for increased model generalization capabilities, its effectiveness when data is limited, and its potential to scale to larger datasets in fingerprint PAD. All collected saliency data and trained models are released with the paper to support reproducible research.

1. Introduction

Fingerprint presentation attack detection (PAD) is an important challenge in biometrics, aimed at distinguishing between genuine fingerprint samples and spoofed (fake) ones. Presentation attacks refer to attempts to deceive fingerprint recognition systems using artificial means, such as synthetic fingerprint impressions made from materials like silicone or gel. Given that fingerprint biometrics are widely employed in systems requiring high levels of security, enhancing their ability to detect spoofing attempts is essential. Deep learning-based fingerprint PAD systems, while effective in detecting known attack types, struggle with generalizing to new or unseen spoofing techniques [17]. These systems are further limited by the scarcity of rarer spoofs, reducing the diversity of known attack types and impacting the ability to evaluate novel ones. This lack of generalization remains a critical issue as fingerprint attack methods continue to evolve rapidly [32].

Saliency-guided training offers a promising solution to the challenges of fingerprint PAD by directing model decision-making to salient regions, focusing learning on discriminative features and on ignoring features accidentally correlated with class labels. Saliency guidance has been applied through both image transformation-based and loss-based approaches, including blurring non-salient regions [2] and aligning Class Activation Mapping (CAM) [38] with salient regions [3], respectively. This technique has been shown to improve model training and convergence,

particularly in scenarios with limited data [18]. Saliency-guided training can also improve model trustworthiness, fairness, and explainability [11].

This paper aims to investigate whether saliency-guided training can improve fingerprint PAD performance by directing model learning to salient fingerprint regions. To explore this intersection, we introduce a dataset of 800 doubly human-annotated saliency maps and text descriptions collected in a 50-participant study, using bonafide and spoof fingerprint samples sourced from previous Fingerprint Liveness Detection Competitions (LivDet) [20, 21, 25, 5]. Additionally, we introduce algorithmically-sourced *pseudosalient* maps, including autoencoder-generated saliency, fingerprint matcher-sourced minutiae-based saliency, and fingerprint image quality-based saliency.

We use all saliency types introduced above in a saliency-guided training paradigm to train fingerprint PAD models and answer the following research questions:

- **RQ1:** Does saliency-guided training with human-annotative saliency improve generalization and classification accuracy for fingerprint PAD?
- **RQ2:** Are algorithmically-sourced pseudosalient types effective for fingerprint PAD?
- **RQ3:** How does saliency-guided training affect fingerprint PAD generalization compared to other biometric attack detection tasks?

Alongside contributions at the intersection of saliency-guided training and fingerprint PAD, this paper releases all explored saliency data at <https://github.com/CVRL/Human-Machine-Pairing-Fingerprint-PAD>, including the 800 doubly human-annotated saliency maps, the various sets of algorithmically-sourced pseudosalient and the trained fingerprint PAD models.

2. Related Work

Presentation attack detection is a lasting challenge within many biometric modalities, including iris [13], face [28, 1], voice [31], or fingerprint [32, 17] recognition systems. Saliency-guided training has been reported to increase generalization in a variety of biometric tasks: iris PAD [2, 10, 12], synthetic face detection [3, 9, 10, 12], and chest X-ray analysis [35, 36]. This section, due to the paper’s goal related to exploration of saliency-based guidance of fingerprint PAD models, will discuss shortly the relevant literature on neural networks-based fingerprint PAD, and applications of saliency in training deep learning models solving biometric PAD tasks.

2.1. Neural Networks for Fingerprint PAD

The Fingerprint Liveness Detection Competition (henceforth referred to as LivDet-Fingerprints), held every other year since 2009 [19], illuminates the state of fingerprint presentation attack detection techniques throughout the years. Deep learning-based submissions first appeared in the 2015 edition of the competition [20]. In LivDet-Fingerprints 2023, the most recent edition of the competition [27], every submission included some form of deep learning. The shift to deep learning can be attributed to the desire for generalization capabilities, since detecting unknown attack types is critical in LivDet competitions. Accordingly, the past five editions of the competition include novel attack types in their unseen testing sets [20, 21, 25, 5, 27].

A common strategy in early neural network-based fingerprint PAD approaches was to analyze the fingerprint in patches, with each patch classification contributing as a vote toward the final decision. Decomposing training samples into multiple smaller patches, particularly from the corners and center, enhances model performance by increasing training diversity [23]. Expanding datasets through patch reflection or normally-distributed random patch selection can also improve generalization [26]. Selecting patches based on the segmented foreground of a fingerprint can provide more relevant discriminatory information [34, 37], while minutiae-based patch selection has been shown to align well with key fingerprint features [6, 7].

Fingerprint PAD research emphasizes strategies for handling and generalizing to unknown presentation attacks [4]. Dynamic adaptation of fingerprint liveness detectors has been described as a way to automatically learn and respond to previously unseen materials [29]. Expanding training data through style-transfer techniques has been demonstrated to improve model robustness against underrepresented attacks [14]. Further, synthetic fingerprint generation via style transfer can diversify training sets without requiring any spoof samples at all [8].

2.2. Saliency Guidance for Biometric PAD

Saliency-guided training primarily involves aligning model decision-making with regions of interest, denoted by saliency maps [3]. Saliency guidance has been shown to enhance model generalization, making it well-suited for biometric PAD tasks [12].

This paper uses CYBORG loss $\mathcal{L}_{\text{CYBORG}}$ [3] as a representative loss for saliency-guided training. It is a two-component loss composed of the classification component $\mathcal{L}_{\text{classification}}$ and the human saliency component $\mathcal{L}_{\text{saliency-guidance}}$, where:

$$\begin{aligned} \mathcal{L}_{\text{CYBORG}} = & \alpha * \mathcal{L}_{\text{classification}} \\ & + (1 - \alpha) * \mathcal{L}_{\text{saliency-guidance}}, \end{aligned} \quad (1)$$

and α weighs the two loss components. When $\alpha = 1.0$, $\mathcal{L}_{\text{CYBORG}}$ becomes a standard cross-entropy loss, and when $\alpha = 0.0$, $\mathcal{L}_{\text{CYBORG}}$ is only penalizing the model for lack of alignment between the model’s and external saliences, regardless of classification performance. In [3], saliency-guidance loss aligns Class Activation Mapping with human-sourced saliency provided for all training samples. By balancing human alignment with classification loss, models are more likely to learn discriminative features from human-salient regions.

Saliency guidance has also been explored in a transformation-based approach. To preserve regions marked as important by provided saliency maps, non-salient unmarked regions are blurred [2]. This process aims to remove any distinguishing features from unannotated regions, effectively forcing model feature learning in areas highlighted by provided saliency maps.

Saliency-guided training has demonstrated significant improvements in model generalization and classification accuracy when guided by both human- and algorithm-sourced saliency. Iris PAD models have benefited from guidance by human annotations [2], AI student-generated saliency [10], autoencoder-generated saliency [12], and iris segmentation saliency [12]. For synthetic face detection, the currently explored saliency types are human annotations [3], AI student-generated saliency [10], autoencoder-generated saliency [12], and face segmentation saliency [12]. For both iris PAD and synthetic face detection, autoencoder-generated saliency, trained to predict human annotations on new samples, is the best explored saliency thus far. To maximize performance using saliency-guided training, the fidelity of conveyed information can be optimized through varying saliency granularities [12].

3. Research Design

Our research design consists of two main components: a human saliency collection study and an exploratory evaluation of saliency-guided fingerprint PAD models, trained with various saliency construction approaches aiming to guide the models towards features that improve generalization against unseen attack types.

3.1. Justification of Data Selection

We use the LivDet-Fingerprint datasets from 2015, 2017, 2019, and 2021 for both saliency collection and saliency-guided training [20, 21, 25, 5]. These datasets were chosen for three key reasons. First, they are the most recent and well-established benchmarks for evaluation of fingerprint PAD available to these authors. Second, their combined use provides a broader range of presentation attack instruments and capture devices, providing greater diversity than any single LivDet-Fingerprint competition alone. Finally, the LivDet-Fingerprint 2021 test set is the most challeng-

ing among our available datasets, as evidenced by its lower reported competitor scores compared to previous available LivDet-Fingerprint test sets. This increased difficulty, along with its inclusion of attack types not present in its training set or any prior LivDet dataset, makes it a strong choice for evaluating model performance.

3.2. Construction of Limited Data Context

The training of biometric PAD models, including fingerprint PAD, is often limited by the availability of high-quality spoof samples [17]. To simulate training conditions under a limited data availability context, we construct an 800-sample training dataset. This dataset size is selected to align with similar studies exploring low-data saliency strategies (*e.g.* 765 in [2]). The limited data context is balanced by class, with 400 bonafide and 400 spoof samples. The spoof samples are further balanced over eight attack types at 50 samples each, sourced from the LivDet-Fingerprint 2015-2019 train and test datasets and the LivDet-Fingerprint 2021 train datasets: Ecoflex [20, 21, 25], gelatine [20, 21, 25], latex [20, 21, 25, 5], liquid Ecoflex [20, 21, 25], woodglue [20, 21, 25], body double [21], mix [25], and RPRO Fast [5]. Bonafide and spoof samples are further balanced by the capture sensors represented by each subclass (note that not all attack types are represented by all scanners).

3.3. Human-Annotative Saliency Collection

Biometric saliency guidance research is based on human-annotative saliency, which, to our knowledge, has not been previously collected for the fingerprint PAD task. To support our exploration and future work in this domain, we conducted an annotation collection study. An example image annotated by a subject to indicate features supporting their decision is illustrated in Fig. 1.

We recruited 50 participants from the University of Notre Dame using a convenience sampling technique due to accessibility, scheduling, and other practical constraints. We collected annotations over the limited 800-sample dataset described in Sec. 3.2. Each participant annotated 32 fingerprint scans, 16 bonafide and 16 spoof samples, with spoof samples spanning eight attack types (two images per type). Participants used an image annotation software specially designed for this study to (a) predict each sample’s class (genuine or fake), (b) annotate salient regions supporting their decision, and (c) optionally provide textual description to further support their classification decisions (*e.g.*, in cases when it would be difficult to support subject’s decision by annotating the image, such as perfect symmetry of the fingerprint image, or unnatural contrast, or too dark image). Participants were not instructed to annotate any specific fingerprint features (*e.g.* whorls, ridges), as intuitively-annotated regions mitigate feature bias, promote straightforward collection reproducibility, and better align with the

philosophy of saliency guidance. The created image annotation software also recorded start and end time stamps of each stroke. This allows for fine-grained analysis of annotation time and provides the order of features annotated by each subject on each sample. Confounding factors in this study include the level of biometric expertise or fingerprint familiarity among annotators. However, we consider this factor to be of limited concern, as prior saliency collection studies have demonstrated success with non-expert annotators [2, 3].

3.4. Construction of Saliency Types

We construct several saliency types for our training experiments, including human-annotated saliency and algorithmically-sourced alternatives, which we term *pseudosalient*. All types of saliency are displayed in Fig. 2.

3.4.1 Human-Annotative Saliency

Human-annotative saliency maps are derived from human annotations collected in the study described in Sec. 3.3. Following established methodology [3], each map is created by averaging the saliency annotations from two independent annotators. We derive three levels of saliency granularity using techniques described in [12]:

- Features of Interest (FOI), the original continuous-valued human-annotative saliency map,
- Area of Interest (AOI), a binarized version of the FOI, and
- Boundary of Interest (BOI), the minimally enclosing rectangle around the AOI.

3.4.2 Pseudosalient Maps

We further produce several types of *pseudosalient*, which we define as saliency that conveys human-interpretable, domain-specific information, but is not directly drawn or labeled by humans.

Minutiae-based pseudosalient maps are constructed from minutiae points extracted using the Neurotechnology VeriFinger 13.1 SDK [22]. Each detected minutia is drawn as a circular region with a radial falloff, using a radius of 10 pixels. FOI, AOI, and BOI granularities are derived using the same transformation process as in human-annotative saliency. The intuition behind this pseudosalient type is that regions considered important for the fingerprint recognition task may translate in importance to fingerprint PAD.

Low-quality pseudosalient maps indicate fingerprint regions with poor pattern fidelity. These are constructed using NBIS-generated quality and low-contrast maps [24].

Specifically, the quality map is inverted to emphasize low-quality areas, the low-contrast map is also inverted to segment the fingerprint pattern, and the final saliency map is obtained by masking the inverted quality map with the inverted low-contrast map. This creation process preserves low-quality regions that lie on the fingerprint pattern. The intuition behind this pseudosalient type is that low-quality regions in the image may reflect poor imitations of genuine fingerprint features, suggesting a possible spoof.

Autoencoder-generated pseudosalient maps are generated to mimic human annotations on unannotated fingerprint samples. We employ a DenseNet-161-based U-Net architecture [30], trained using human-annotated samples, following prior autoencoder-based strategy [12]. The resulting maps are treated as FOI-level saliency. AOI is obtained by thresholding at 0.5 to account for autoencoder artifacts, and BOI is computed by minimally enclosing AOI.

3.5. Training of PAD Models and Metrics Used

To select model training configurations, we used maximum variation purposive sampling to account for variations in saliency types, loss balancing weights, model architectures, and data contexts. The data collection technique is indirect, involving analysis of usage logs: each model’s predictions on a shared testing set (the LivDet-Fingerprint 2021 testing set). The primary metrics of analysis are each model’s testing classification accuracy at the validation Equal Error Rate-equivalent threshold and Area Under the ROC curve (AUC). Key confounding factors in evaluating machine learning models include class imbalance and overfitting. We mitigate these by balancing training data (ensuring equal distribution of bona fide/spoof samples, attack types, and scanner types) and testing on unseen data that includes novel attack types.

4. Experimental Training Scenarios

To assess the impact of saliency-guided training on fingerprint PAD, we designed a series of training scenarios that explore different model configurations under varying data availability constraints and saliency integration methods. These experiments compare saliency-guided configurations against both baseline techniques and each other, given the sensitivity of saliency guidance to implementation choices.

All models are evaluated on LivDet-Fingerprint 2021 testing set, which contains novel attack types, was never used in training, and enables direct comparison with algorithms submitted to the competition. Further, we train each configuration on three convolutional neural network (CNN) architectures: ResNet50 [15], DenseNet-121 [16], and Inception-V3 [33]. Each configuration undergoes three independent training runs to assess the variability of point error estimates (accuracy and AUC). All training and testing

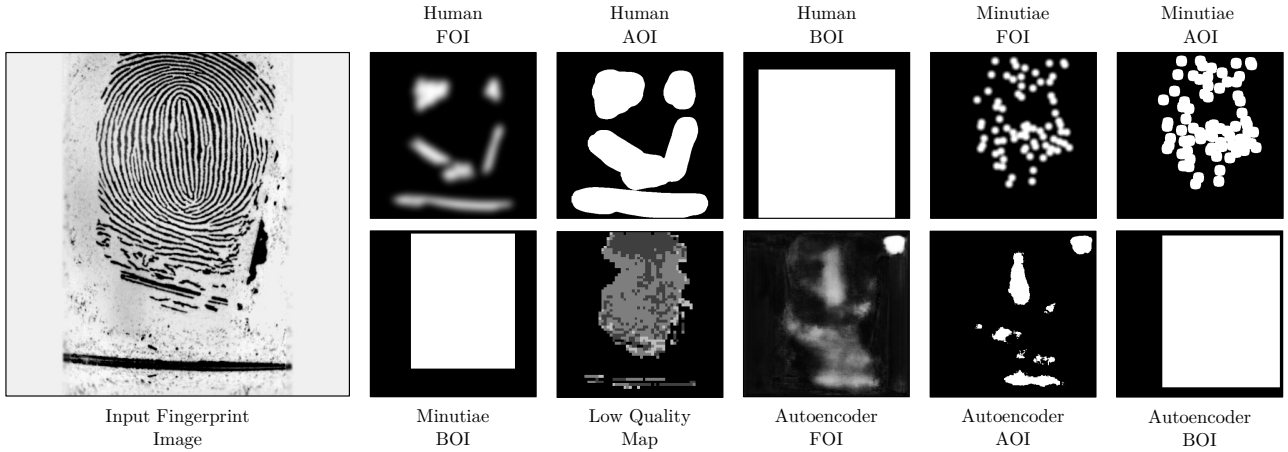


Figure 2. Illustration of all saliency types explored in our saliency-guided training experiments for an example fingerprint image. FOI, AOI, and BOI refer to Features-, Area-, and Boundary of Interest saliency granularities, respectively.

samples are center-cropped and resized to 224×224 pixel resolution.

4.1. Scenario S1: Large Data Baseline

To establish a benchmark under large data availability conditions, we train models on a comprehensive dataset containing all available LivDet-Fingerprint samples (certainly excluding the LivDet-Fingerprint 2021 test set), totaling 59,792 fingerprint images. Validation is randomly selected at 20%, and the models are trained using cross-entropy loss, hence without any saliency guidance.

4.2. Scenario S2: Limited Data Baseline

To simulate limited-data conditions, typical for PAD problems, we train models on a reduced 800-sample dataset (the same dataset used for human-annotative saliency collection) using cross-entropy loss. Again, no saliency information is used to guide the models during training. This scenario highlights the challenges of learning from limited spoof samples and serves as a baseline for saliency-guided methods.

4.3. Scenario S3: Limited Data Availability with Loss-Based Saliency-Guidance

Using the same 800-sample dataset as in S2, but now with saliency information, we implement saliency guidance via the CYBORG loss function [3], which aligns model’s Class Activation Maps with external saliency during training to encourage learning in relevant regions. To explore the effect of saliency weighting, we experiment with different values of the CYBORG loss weighting parameter α , which determines the proportion of cross-entropy loss versus saliency alignment loss. Specifically,

we test $\alpha = \{0.1, 0.3, 0.5, 0.7, 0.9\}$, covering a wide range from heavily CAM-alignment training to predominantly cross-entropy-based learning. We evaluate on the following saliency types, defined in Sec. 3.4: human-annotative saliency (FOI, AOI, BOI), minutiae-based pseudosalienty (FOI, AOI, BOI), and low-quality pseudosalienty.

4.4. Scenario S4: Limited Data Availability with Blur-Based Saliency Guidance

Following the same 800-sample dataset structure, we apply saliency guidance with cross-entropy loss through a transformation-based strategy [2], where non-salient regions are Gaussian blurred (radii = {2, 4, 6, 8, 10, 12, 14, 16}) to “remove” (by blurring) irrelevant and emphasize important features, increasing the effective training set size eightfold. To mitigate edge artifacts between blurred and unblurred regions, the saliency masks are smoothed with a Gaussian blur (radius = 5). We explore the same saliency types as those used in scenario S3.

As a control, we train models on fully blurred images at the same radii, alongside the original unblurred images, expanding the training set ninefold. This ensures that observed performance differences are from retained salient regions rather than dataset generic (non-saliency-related) augmentations.

4.5. Scenario S5: Large Data Availability with Loss-Based Pseudosalienty Guidance

Using the autoencoder-generated pseudosalienty process described in Sec. 3.4, we generate FOI, AOI, and BOI pseudosalienty for the large data (omitting the 800 human-annotated samples used to train the autoencoder). We further produce minutiae-based (FOI, AOI, and BOI) and quality-based pseudosalienty for the expanded data. This

Saliency	Granularity	Network	Loss	α	Accuracy	Bonafide Acc.	Spoof Acc.	AUC
S1: Large Data Baseline								
-	-	ResNet	Cross Entropy	-	0.911 \pm 0.001	0.995 \pm 0.000	0.821 \pm 0.003	0.989 \pm 0.000
S2: Limited Data Baseline								
-	-	Inception	Cross Entropy	-	0.862 \pm 0.010	0.948 \pm 0.009	0.769 \pm 0.014	0.946 \pm 0.007
S3: Limited Data Availability with Loss-Based Saliency Guidance								
Human	AOI	Inception	CYBORG	0.9	0.879 \pm 0.006	<u>0.966\pm0.002</u>	0.786 \pm 0.012	0.959 \pm 0.002
Minutiae	FOI	Inception	CYBORG	0.7	<u>0.885\pm0.004</u>	0.952 \pm 0.006	<u>0.812\pm0.014</u>	0.961 \pm 0.004
Low Quality	-	Inception	CYBORG	0.5	0.876 \pm 0.011	0.953 \pm 0.014	0.795 \pm 0.019	0.951 \pm 0.005
S4: Limited Data Availability with Blur-Based Saliency Guidance								
-	-	Inception	Cross Entropy	-	0.794 \pm 0.018	0.869 \pm 0.019	0.714 \pm 0.057	0.878 \pm 0.013
Human	BOI	Inception	Cross Entropy	-	<u>0.873\pm0.006</u>	<u>0.958\pm0.007</u>	0.781 \pm 0.015	<u>0.953\pm0.004</u>
Minutiae	AOI	Inception	Cross Entropy	-	0.868 \pm 0.008	0.907 \pm 0.008	<u>0.825\pm0.020</u>	0.942 \pm 0.006
Low Quality	-	Inception	Cross Entropy	-	0.828 \pm 0.018	0.843 \pm 0.020	0.813 \pm 0.019	0.906 \pm 0.016
S5: Large-Data Availability with Pseudosaliency Guidance								
Autoencoder	AOI	Inception	CYBORG	0.9	0.916 \pm 0.011	0.994 \pm 0.001	0.831 \pm 0.024	0.990\pm0.001
Minutiae	AOI	DenseNet	CYBORG	0.9	0.938\pm0.004	0.964 \pm 0.001	0.910\pm0.009	0.988 \pm 0.001
Low Quality	-	Inception	CYBORG	0.9	0.906 \pm 0.011	0.996\pm0.001	0.808 \pm 0.023	0.808 \pm 0.023

Table 1. Summary of best-accuracy-achieving configurations across five training scenarios. Each row describes a configuration as well as its key performance metrics. For each metric, the highest inter-scenario score is **bolded** and the highest intra-scenario score is underlined. Full scenario results are available in the supplementary materials.

scenario evaluates whether non-human pseudosaliency can effectively scale saliency-guided training to larger datasets.

5. Results

This section presents the results of the five training scenarios by directly addressing the research questions listed in Sec. 1. A summary of the top-performing configurations for each scenario is provided in Tab. 1.

Addressing RQ1: Does saliency-guided training with human-annotative saliency improve generalization and classification accuracy?

Model training with human saliency is explored in scenarios S3 and S4, and its best configurations are described in Tab. 1. In both loss- and blur-based saliency guidance, human-guided configurations outperform their comparative limited-data baselines (scenarios S2 and S4).

Among human-saliency configurations with limited-data loss-based guidance (scenario S3), the configuration achieving the highest accuracy is configured with the Area of Interest saliency granularity, the Inception architecture, and a CYBORG α weight of 0.9. Its achieved accuracy of 0.879 ± 0.006 and AUC of 0.959 ± 0.002 outperform the best baseline configuration (scenario S2) by 0.017 and 0.013, respectively.

Continually, the best human saliency blur-guided model (scenario S4), using the Boundary of Interest granularity and the Inception architecture, achieves a classification accuracy of 0.873 ± 0.006 and an AUC of 0.953 ± 0.004 , surpassing the blurring baseline by 0.079 and 0.075, respectively.

These results demonstrate that **saliency-guided training with human-annotative saliency improves generalization and classification accuracy for fingerprint PAD**.

Addressing RQ2: Are algorithmically-sourced pseudosaliency types effective for saliency-guided training of fingerprint PAD?

Table 1 outlines the best training configurations for pseudosaliency-guided models, as explored in scenarios S3, S4, and S5. In the limited data context, all explored pseudosaliency types, when optimally configured, are capable of outperforming baseline models (scenarios S2 and S4). In the large-data context, two of the three proposed pseudosaliency types exceed baseline performance (scenario S1).

For loss-based pseudosaliency guidance in the limited-data context (scenario S3), minutiae-based Features of Interest saliency type achieves the highest classification accuracy (0.885 ± 0.004) and AUC (0.961 ± 0.004), surpassing the baseline metrics (scenario S2) by 0.023 in accuracy, and

Domain	Baseline	Saliency-Guided Training	Normalized Gain
Iris PAD [12]	0.893 \pm 0.019	0.962 \pm 0.005	+64.5%
Synthetic Face Detection [12]	0.572 \pm 0.047	0.643 \pm 0.033	+16.6%
Fingerprint PAD (limited)	0.946 \pm 0.007	0.961 \pm 0.004	+27.8%
Fingerprint PAD (large)	0.990 \pm 0.001	0.991 \pm 0.001	+10.0%

Table 2. Normalized generalization gain of the highest-AUC-scoring saliency-guided models across four biometric attack detection tasks.

by 0.015 in AUC. This is the best performance exhibited in the limited data context, outperforming human-annotative saliency.

For blur-based guidance (scenario S4), the best pseudosalienty-guided model uses the minutiae-based Area of Interest saliency type, achieving a classification accuracy of 0.868 \pm 0.008 and an AUC of 0.942 \pm 0.006, outperforming the blurring baseline but not the best human saliency configuration.

The generative nature of pseudosalienty enables saliency-guided training to scale effectively in larger data availability contexts, as explored in scenario S5. The best configuration in this scenario employs minutiae-based Area of Interest pseudosalienty, achieving an accuracy of 0.938 \pm 0.004. This result outperforms the large-data baseline (scenario S1) by 0.027. When compared to the reported LivDet-Fingerprint 2021 rankings [5], **this performance would have earned or tied for first place**, accounting for our reported standard deviation (which was not included in the LivDet-Fingerprint 2021 results). This configuration raises spoof detection accuracy by 8.9%, demonstrating the generalization strength of saliency-guided training.

Thus, we can affirm that **algorithmically-sourced pseudosalienty is effective for saliency-guided fingerprint PAD training**. Moreover, it is capable of exceeding human-annotative saliency performance as well as scaling to large data contexts, even if not directly designed for the fingerprint PAD task.

Addressing RQ3: How does saliency-guided training affect fingerprint PAD generalization compared to other biometric attack detection tasks?

As in answers to the research questions RQ1 and RQ2, saliency-guided training enhances both generalization and classification performance for fingerprint PAD, further affirming its applicability to biometric attack detection tasks. However, comparing performance across domains requires understanding baseline differences. Considering achieved AUC, fingerprint PAD baselines already perform relatively well compared to iris presentation attack detection and synthetic face detection [2, 3, 12], meaning there is less room for improvement.

To evaluate the impact of saliency-guided training on model generalization while accounting for baseline perfor-

mance, we compute normalized gain g , defined for a metric M as:

$$g_{\text{normalized}} = \frac{M_{\text{saliency-guided}} - M_{\text{baseline}}}{100\% - M_{\text{baseline}}} \quad (2)$$

Tab. 2 summarizes normalized AUC performance gains for iris PAD, synthetic face detection, and fingerprint PAD in both large and limited data contexts. The generalization gains observed for fingerprint PAD are most comparable to those in synthetic face detection but less than improvements in iris PAD, as reported in [12]. Thus, we conclude that **saliency-guided training positively impacts fingerprint PAD generalization to a similar or lesser extent than other biometric domains**.

6. Discussion

Through our explored scenarios and answered research questions, we provide a foundational understanding of saliency-guided training for fingerprint PAD. In this section, we will highlight key observations and broader takeaways from our findings.

6.1. Improvements to Bonafide vs. Spoof Accuracy

A closer look at model performance metrics in Tab. 1 reveals that saliency-guided training primarily raises spoof detection accuracy, with bonafide accuracy usually affected to a lesser degree. In the limited-data context, the best configuration (Inception, CYBORG, $\alpha=0.7$, Minutiae FOI) improves spoof accuracy by 4.3%, while bonafide accuracy increases by only 0.4%. Similarly, in the large-data context, the best configuration (DenseNet, CYBORG, $\alpha=0.9$, Minutiae AOI) gains 8.9% in spoof accuracy but loses 3.1% in bonafide accuracy.

6.2. CNN Architecture Sensitivity

We observe patterns among high-performing configurations that suggest broader trends in saliency-guided training for fingerprint PAD. Notably, the Inception-V3 architecture consistently performs well, appearing in all but two top-accuracy-achieving models across best explored configurations described in Tab. 1. This contrasts with other explored biometric attack detection tasks: DenseNet performs best on average for iris PAD, while ResNet and DenseNet

alternate depending on loss in synthetic face detection [12]. These results indicate that there is no optimal architecture for saliency-guided training across biometric PAD domains. This further describes how this training paradigm is highly sensitive to configuration, including saliency type and granularity, loss weighting, and size of training data.

6.3. Blurring and BOI Saliency Granularity

In blur-based saliency guidance, the Boundary of Interest (BOI) saliency granularity consistently performs well. It is the best granularity for human saliency and second best among explored pseudosalient types. BOI saliency identifies a minimal enclosing rectangle around all regions of interest, which typically encompasses most of the fingerprint area. Consequently, when non-salient regions are blurred, the fingerprint pattern remains largely unaffected. Combined with eightfold data augmentation through multiple blur radii, the model encounters the nearly unblurred pattern repeatedly. This inadvertently increases exposure to samples during training, similar to training with standard cross entropy for many additional epochs. While BOI saliency achieves high scores on key metrics, this effectiveness is likely due to unintended augmentation behavior rather than true saliency-based guidance, which impacts how blur-based saliency guidance results may be interpreted.

6.4. Effectiveness of Pseudosalient Types

Software-generated pseudosalient, specifically minutiae- and low-quality-based types, proved effective for fingerprint PAD guidance. Models trained with these sources matched or exceeded the performance of those trained with human-annotative saliency (scenario S3). This contrasts with prior findings in other biometric domains [12], where image segmentation-based saliency for iris and face images resulted in sub-baseline performance for both iris PAD and synthetic face detection. Autoencoder-generated pseudosalient also proved effective for fingerprint PAD (scenario S5), outperforming the baseline in the large-data scenario (scenario S1). This is consistent with previous findings where autoencoder-based saliency surpassed human annotations in both iris and face domains [12].

From these results, we hypothesize that effective pseudosalient must communicate domain-specific knowledge. Minutiae-based saliency highlights distinguishing fingerprint features used in recognition. Low-quality maps carry meaningful information about a fingerprint’s fidelity. Autoencoder-generated saliency is inspired by human annotation training data collected directly for the fingerprint PAD task. In contrast, image segmentation models simply describe object boundaries without offering domain-specific insights. Our findings suggest that algorithmically-

sourced pseudosalient maps, when grounded in domain-specific knowledge, offer a scalable and cost-effective alternative to human annotations, particularly when human annotations are difficult or expensive to obtain.

6.5. Scalability and Future Directions of Saliency-Guided Training

Scenario S5 offers a promising insight into the potential scalability of saliency-guided training. Prior work has shown that while saliency-guided training can provide gains in limited-data contexts, it typically fails to surpass performance achieved with large-scale training alone [2]. Our results in limited-data scenarios (S2, S3, S4) reflect this trend. However, by incorporating generative pseudosalient in a large-data context (scenario S5), we observe accuracy and generalization improvements over the large-data baseline (scenario S1) across several configurations.

The results of scenario S5 represent a meaningful step forward: it suggests that generative saliency approaches may help scale saliency-guided training to previously inapplicable large datasets. These findings point toward future directions where pseudosalient guidance at-scale could positively complement traditional training.

7. Conclusion

This paper explores the intersection of saliency-guided training and fingerprint presentation attack detection, examining how saliency types, guidance strategies, and data availability contexts influence model behavior. Across five experimental scenarios, for the first time we evaluate the impact of human-annotative saliency and algorithmically-sourced pseudosalient in guiding the training of fingerprint PAD models. Our findings reveal meaningful benefits in classification and generalization performance, though to a lesser extent than in other biometric domains. We highlight the configuration-sensitive nature of saliency-guided training and identify promising directions for scalable, domain-aware saliency generation.

To support future research and facilitate full replicability of this study, we release both human-annotated saliency and algorithmically-sourced pseudosalient data, along with source codes and model weights. Overall, this work contributes to a deeper understanding of how saliency-guided training strategies behave within the fingerprint PAD domain.

Acknowledgment This material is based upon work supported by the U.S. National Science Foundation under grant No. 2237880. Any opinions, findings, conclusions, or recommendations expressed in this material are those of the author(s) and do not necessarily reflect the views of the U.S. National Science Foundation.

References

- [1] S. Bhattacharjee, A. Mohammadi, A. Anjos, and S. Marcel. Recent advances in face presentation attack detection. *Handbook of biometric anti-spoofing: presentation attack detection*, pages 207–228, 2019. [2](#)
- [2] A. Boyd, K. Bowyer, and A. Czajka. Human-aided saliency maps improve generalization of deep learning, 2021. [1, 2, 3, 4, 5, 7, 8](#)
- [3] A. Boyd, P. Tinsley, K. W. Bowyer, and A. Czajka. Cyborg: Blending human saliency into the loss improves deep learning-based synthetic face detection. In *Proceedings of the IEEE/CVF Winter Conference on Applications of Computer Vision*, pages 6108–6117, 2023. [1, 2, 3, 4, 5, 7](#)
- [4] S. Carta, R. Casula, G. Orrù, M. Micheletto, and G. L. Marcialis. Interpretability of fingerprint presentation attack detection systems: a look at the “representativeness” of samples against never-seen-before attacks. *Machine Vision and Applications*, 36(2):44, 2025. [2](#)
- [5] R. Casula, M. Micheletto, G. Orrù, R. Delussu, S. Concas, A. Panzino, and G. L. Marcialis. Livdet 2021 fingerprint liveness detection competition-into the unknown. In *2021 IEEE international joint conference on biometrics (IJCB)*, pages 1–6. IEEE, 2021. [2, 3, 7](#)
- [6] T. Chugh, K. Cao, and A. K. Jain. Fingerprint spoof detection using minutiae-based local patches. In *2017 IEEE International Joint Conference on Biometrics (IJCB)*, pages 581–589. IEEE, 2017. [2](#)
- [7] T. Chugh, K. Cao, and A. K. Jain. Fingerprint spoof buster: Use of minutiae-centered patches. *IEEE Transactions on Information Forensics and Security*, 13(9):2190–2202, 2018. [2](#)
- [8] T. Chugh and A. K. Jain. Fingerprint spoof detector generalization. *IEEE Transactions on Information Forensics and Security*, 16:42–55, 2020. [2](#)
- [9] C. Crum, P. Tinsley, A. Boyd, J. Piland, C. Sweet, T. Kelley, K. Bowyer, and A. Czajka. Explain to me: Salience-based explainability for synthetic face detection models, 2023. [2](#)
- [10] C. R. Crum, A. Boyd, K. Bowyer, and A. Czajka. Teaching ai to teach: Leveraging limited human salience data into unlimited saliency-based training. *arXiv preprint arXiv:2306.05527*, 2023. [2, 3](#)
- [11] C. R. Crum and C. Coglianese. Taking training seriously: Human guidance and management-based regulation of artificial intelligence. In *2024 International Joint Conference on Neural Networks (IJCNN)*, pages 1–9. IEEE, 2024. [2](#)
- [12] C. R. Crum, S. Webster, and A. Czajka. Grains of saliency: Optimizing saliency-based training of biometric attack detection models, 2024. [2, 3, 4, 7, 8](#)
- [13] A. Czajka and K. W. Bowyer. Presentation attack detection for iris recognition: An assessment of the state-of-the-art. *ACM Computing Surveys (CSUR)*, 51(4):1–35, 2018. [2](#)
- [14] R. Gajawada, A. Popli, T. Chugh, A. Namboodiri, and A. K. Jain. Universal material translator: Towards spoof fingerprint generalization. In *2019 International Conference on Biometrics (ICB)*, pages 1–8. IEEE, 2019. [2](#)
- [15] K. He, X. Zhang, S. Ren, and J. Sun. Deep residual learning for image recognition. *corr abs/1512.03385* (2015), 2015. [4](#)
- [16] G. Huang, Z. Liu, L. Van Der Maaten, and K. Q. Weinberger. Densely connected convolutional networks. In *Proceedings of the IEEE conference on computer vision and pattern recognition*, pages 4700–4708, 2017. [4](#)
- [17] K. Karampidis, M. Rousouliotis, E. Linardos, and E. Kavalieratou. A comprehensive survey of fingerprint presentation attack detection. *Journal of Surveillance, Security and Safety*, 2(4):117–161, 2021. [1, 2, 3](#)
- [18] D. Linsley, D. Shiebler, S. Eberhardt, and T. Serre. Learning what and where to attend, 2019. [2](#)
- [19] G. L. Marcialis and F. Roli. Liveness detection competition 2009. *Biometric Technology Today*, 17(3):7–9, 2009. [2](#)
- [20] V. Mura, L. Ghiani, G. L. Marcialis, F. Roli, D. A. Yambay, and S. A. Schuckers. Livdet 2015 fingerprint liveness detection competition 2015. In *2015 IEEE 7th International Conference on Biometrics Theory, Applications and Systems (BTAS)*, pages 1–6, 2015. [2, 3](#)
- [21] V. Mura, G. Orrù, R. Casula, A. Sibiri, G. Loi, P. Tuveri, L. Ghiani, and G. L. Marcialis. Livdet 2017 fingerprint liveness detection competition 2017. In *2018 international conference on biometrics (ICB)*, pages 297–302. IEEE, 2018. [2, 3](#)
- [22] Neurotechnology. Verifinger sdk. [4](#)
- [23] R. F. Nogueira, R. de Alencar Lotufo, and R. C. Machado. Fingerprint liveness detection using convolutional neural networks. *IEEE transactions on information forensics and security*, 11(6):1206–1213, 2016. [2](#)
- [24] N. I. of Standards and Technology. Nist biometric image software (nbis). [4](#)
- [25] G. Orrù, R. Casula, P. Tuveri, C. Bazzoni, G. Dessalvi, M. Micheletto, L. Ghiani, and G. L. Marcialis. Livdet in action-fingerprint liveness detection competition 2019. In *2019 international conference on biometrics (ICB)*, pages 1–6. IEEE, 2019. [2, 3](#)
- [26] E. Park, W. Kim, Q. Li, J. Kim, and H. Kim. Fingerprint liveness detection using cnn features of random sample patches. In *2016 International Conference of the Biometrics Special Interest Group (BIOSIG)*, pages 1–4, 2016. [2](#)
- [27] S. Purnapatra, H. Rezaie, B. Jawade, Y. Liu, Y. Pan, L. Brosell, M. R. Sumi, L. Igene, A. Dimarco, S. Setlur, et al. Liveness detection competition-noncontact-based fingerprint algorithms and systems (livdet-2023 noncontact fingerprint). In *2023 IEEE International Joint Conference on Biometrics (IJCB)*, pages 1–10. IEEE, 2023. [2](#)
- [28] R. Ramachandra and C. Busch. Presentation attack detection methods for face recognition systems: A comprehensive survey. *ACM Computing Surveys (CSUR)*, 50(1):1–37, 2017. [2](#)
- [29] A. Rattani and A. Ross. Automatic adaptation of fingerprint liveness detector to new spoof materials. In *IEEE International Joint Conference on Biometrics*, pages 1–8. IEEE, 2014. [2](#)
- [30] O. Ronneberger, P. Fischer, and T. Brox. U-net: Convolutional networks for biomedical image segmentation. In *Medical image computing and computer-assisted intervention–MICCAI 2015: 18th international conference, Munich, Germany, October 5–9, 2015, proceedings, part III* 18, pages 234–241. Springer, 2015. [4](#)

- [31] M. Sahidullah, H. Delgado, M. Todisco, A. Nautsch, X. Wang, T. Kinnunen, N. Evans, J. Yamagishi, and K.-A. Lee. Introduction to voice presentation attack detection and recent advances. *Handbook of Biometric Anti-Spoofing: Presentation Attack Detection and Vulnerability Assessment*, pages 339–385, 2023. [2](#)
- [32] C. Sousedik and C. Busch. Presentation attack detection methods for fingerprint recognition systems: a survey. *Iet Biometrics*, 3(4):219–233, 2014. [1](#), [2](#)
- [33] C. Szegedy, S. Ioffe, V. Vanhoucke, and A. Alemi. Inception-v4, inception-resnet and the impact of residual connections on learning. In *Proceedings of the AAAI conference on artificial intelligence*, volume 31, 2017. [4](#)
- [34] A. Toosi, S. Cumani, A. Bottino, et al. Cnn patch-based voting for fingerprint liveness detection. In *IJCCI*, pages 158–165, 2017. [2](#)
- [35] T. van Sonsbeek, X. Zhen, D. Mahapatra, and M. Worring. Probabilistic integration of object level annotations in chest x-ray classification, 2022. [2](#)
- [36] B. Wang, H. Pan, A. Aboah, Z. Zhang, E. Keles, D. Torigian, B. Turkbey, E. Krupinski, J. Udupa, and U. Bagci. Gazegnn: A gaze-guided graph neural network for chest x-ray classification, 2023. [2](#)
- [37] Y. Zhang, D. Shi, X. Zhan, D. Cao, K. Zhu, and Z. Li. Slim-rescnn: A deep residual convolutional neural network for fingerprint liveness detection. *IEEE Access*, 7:91476–91487, 2019. [2](#)
- [38] B. Zhou, A. Khosla, A. Lapedriza, A. Oliva, and A. Torralba. Learning deep features for discriminative localization. In *Proceedings of the IEEE conference on computer vision and pattern recognition*, pages 2921–2929, 2016. [1](#)

Appendix

The Appendix contains the complete experimental results for all five training scenarios (S1–S5) explored in the main paper. Each table reports fingerprint PAD model performance across different saliency types, saliency granularities, and network architectures. All configurations are averaged over three independent runs. All testing accuracy metrics are computed using the Equal Error Rate threshold from each model’s validation set predictions. We define all listed columns as:

- **Network:** The CNN network architecture used from: ResNet50, DenseNet-121, and Inception-V3.
- **Alpha (α):** Refers to the α parameter of \mathcal{L}_{CYBORG} loss, which weighs the $\mathcal{L}_{\text{classification}}$ and $\mathcal{L}_{\text{saliency-guidance}}$ parameters. At 0.0, loss is saliency guidance only, and at 1.0, loss is cross entropy only.
- **AUC:** Area under the receiver operating characteristic (ROC) curve.
- **Accuracy:** Overall classification accuracy on the LivDet-Fingerprint 2021 test set.
- **Bonafide Accuracy:** Classification accuracy on bonafide (live, real) fingerprint samples from the LivDet-Fingerprint 2021 test set.
- **Spoof Accuracy:** Classification accuracy on spoof (fake) fingerprint samples from the LivDet-Fingerprint 2021 test set.
- **Placement:** A hypothetical ranking in the LivDet-Fingerprint 2021 competition based on model-achieved Accuracy and reported competitor-achieved accuracies. The placement range is computed over $\mu_{\text{accuracy}} \pm \sigma_{\text{accuracy}}$.
- **d^* :** Measures how well models can distinguish between the live and spoof classes. Higher values indicate greater separability.
- **FNR @ FPR = 1%:** The False Negative Rate at the threshold where the False Positive Rate is 1%. Lower value is better.
- **Attack Type^{U/K} Accuracy:** Classification accuracy across the various spoof (fake) types in the LivDet-Fingerprint 2021 test set. A superscript ^U indicates an unknown attack type (no samples of this attack type seen during training) while a superscript ^K indicates a known attack type (samples of this attack type seen during training).

A. Scenario S1, Full Results

Network	AUC	Accuracy	Bonafide Accuracy	Spoof Accuracy	Placement	d^*	FNR @ FPR = 1%	GLS20 ^U Accuracy	VBN ^U Accuracy	RFastPro ^U Accuracy	Wood Glue ^K Accuracy	Body Double ^K Accuracy
ResNet	0.989±0.000	0.911±0.001	0.995±0.000	0.821±0.003	4	3.261±0.020	0.133±0.004	0.747±0.007	0.893±0.004	0.780±0.003	0.890±0.020	0.868±0.004
DenseNet	0.990±0.001	0.905±0.003	0.995±0.001	0.808±0.006	4	3.317±0.045	0.146±0.010	0.725±0.008	0.898±0.001	0.751±0.004	0.899±0.023	0.857±0.014
Inception	0.990±0.010	0.911±0.008	0.996±0.001	0.819±0.018	3-4	3.273±0.072	0.137±0.006	0.731±0.035	0.914±0.017	0.757±0.045	0.904±0.017	0.884±0.009

Table 3. **Results for Scenario 1.** Models trained using cross entropy in the large-data-availability context. Averaged over three runs.

B. Scenario S2, Full Results

Network	AUC	Accuracy	Bonafide Accuracy	Spoof Accuracy	Placement	d^*	FNR @ FPR = 1%	GLS20 ^U Accuracy	VBN ^U Accuracy	RFastPro ^U Accuracy	Wood Glue ^K Accuracy	Body Double ^K Accuracy
ResNet	0.930±0.003	0.847±0.003	0.928±0.007	0.760±0.014	5	2.093±0.027	0.525±0.042	0.747±0.007	0.893±0.004	0.780±0.003	0.890±0.020	0.868±0.004
DenseNet	0.918±0.016	0.839±0.012	0.944±0.004	0.725±0.025	5	1.978±0.161	0.518±0.063	0.725±0.008	0.898±0.001	0.751±0.004	0.899±0.023	0.857±0.014
Inception	0.946±0.007	0.862±0.010	0.948±0.009	0.769±0.014	5	2.283±0.094	0.474±0.027	0.731±0.035	0.914±0.017	0.757±0.045	0.904±0.017	0.884±0.009

Table 4. **Results for Scenario 2.** Models trained using cross entropy in the limited-data context. Averaged over three runs.

C. Scenario S3, Full Results

Network	Alpha (α)	AUC	Accuracy	Bonafide Accuracy	Spoofer Accuracy	Placement	d'	FNR @ FPR = 1%	GLS20 ^U Accuracy	VBN ^U Accuracy	RFastPro ^U Accuracy	Wood Glue ^K Accuracy	Body Double ^K Accuracy
ResNet	0.9	0.936 \pm 0.006	0.860 \pm 0.012	0.934 \pm 0.011	0.779 \pm 0.035	4-5	2.153 \pm 0.068	0.510 \pm 0.043	0.696 \pm 0.058	0.872 \pm 0.015	0.733 \pm 0.056	0.845 \pm 0.030	0.836 \pm 0.007
DenseNet		0.944 \pm 0.005	0.861 \pm 0.009	0.952 \pm 0.008	0.763 \pm 0.012	5	2.254 \pm 0.057	0.448 \pm 0.039	0.679 \pm 0.025	0.825 \pm 0.052	0.719 \pm 0.015	0.825 \pm 0.025	0.842 \pm 0.009
Inception		0.953 \pm 0.003	0.872 \pm 0.003	0.957 \pm 0.003	0.780 \pm 0.004	4-5	2.365 \pm 0.037	0.446 \pm 0.008	0.705 \pm 0.013	0.863 \pm 0.026	0.736 \pm 0.023	0.831 \pm 0.068	0.841 \pm 0.010
ResNet	0.7	0.932 \pm 0.006	0.850 \pm 0.010	0.942 \pm 0.010	0.751 \pm 0.022	5	2.116 \pm 0.063	0.526 \pm 0.034	0.642 \pm 0.024	0.865 \pm 0.014	0.691 \pm 0.036	0.838 \pm 0.016	0.827 \pm 0.019
DenseNet		0.936 \pm 0.004	0.847 \pm 0.002	0.943 \pm 0.007	0.743 \pm 0.008	5	2.149 \pm 0.050	0.512 \pm 0.027	0.642 \pm 0.034	0.844 \pm 0.016	0.688 \pm 0.031	0.795 \pm 0.033	0.840 \pm 0.024
Inception		0.952 \pm 0.003	0.872 \pm 0.003	0.952 \pm 0.004	0.785 \pm 0.010	4-5	2.360 \pm 0.041	0.482 \pm 0.061	0.697 \pm 0.011	0.877 \pm 0.017	0.734 \pm 0.014	0.857 \pm 0.046	0.846 \pm 0.026
ResNet	0.5	0.920 \pm 0.005	0.835 \pm 0.005	0.928 \pm 0.007	0.735 \pm 0.017	5	1.992 \pm 0.048	0.585 \pm 0.027	0.620 \pm 0.034	0.871 \pm 0.017	0.662 \pm 0.033	0.844 \pm 0.008	0.801 \pm 0.004
DenseNet		0.933 \pm 0.006	0.852 \pm 0.010	0.938 \pm 0.013	0.760 \pm 0.028	5	2.116 \pm 0.064	0.566 \pm 0.045	0.644 \pm 0.053	0.879 \pm 0.011	0.684 \pm 0.042	0.878 \pm 0.018	0.836 \pm 0.029
Inception		0.954 \pm 0.005	0.864 \pm 0.014	0.954 \pm 0.007	0.767 \pm 0.037	4-5	2.387 \pm 0.070	0.480 \pm 0.019	0.659 \pm 0.064	0.889 \pm 0.016	0.705 \pm 0.061	0.854 \pm 0.037	0.838 \pm 0.019
ResNet	0.3	0.901 \pm 0.006	0.820 \pm 0.004	0.902 \pm 0.013	0.731 \pm 0.009	5-7	1.823 \pm 0.051	0.689 \pm 0.045	0.592 \pm 0.020	0.885 \pm 0.023	0.629 \pm 0.019	0.872 \pm 0.034	0.833 \pm 0.019
DenseNet		0.915 \pm 0.010	0.830 \pm 0.014	0.927 \pm 0.001	0.724 \pm 0.029	5-7	1.945 \pm 0.093	0.596 \pm 0.011	0.602 \pm 0.029	0.869 \pm 0.028	0.642 \pm 0.045	0.891 \pm 0.017	0.760 \pm 0.029
Inception		0.945 \pm 0.004	0.861 \pm 0.006	0.938 \pm 0.007	0.778 \pm 0.020	5	2.267 \pm 0.050	0.555 \pm 0.056	0.688 \pm 0.044	0.869 \pm 0.012	0.737 \pm 0.030	0.833 \pm 0.016	0.846 \pm 0.013
ResNet	0.1	0.862 \pm 0.012	0.776 \pm 0.013	0.878 \pm 0.013	0.665 \pm 0.016	7-10	1.540 \pm 0.079	0.689 \pm 0.045	0.592 \pm 0.020	0.885 \pm 0.023	0.629 \pm 0.019	0.836 \pm 0.026	0.750 \pm 0.011
DenseNet		0.872 \pm 0.014	0.787 \pm 0.014	0.889 \pm 0.010	0.677 \pm 0.028	7-9	1.607 \pm 0.093	0.762 \pm 0.028	0.539 \pm 0.034	0.871 \pm 0.026	0.566 \pm 0.028	0.889 \pm 0.031	0.700 \pm 0.022
Inception		0.926 \pm 0.006	0.844 \pm 0.007	0.899 \pm 0.008	0.784 \pm 0.011	5	2.044 \pm 0.056	0.671 \pm 0.030	0.701 \pm 0.026	0.876 \pm 0.006	0.743 \pm 0.020	0.897 \pm 0.019	0.794 \pm 0.011

Table 5. Results for Scenario S3 using human-annotated FOI saliency. Models trained using CYBORG loss in the limited-data context. Averaged over three runs.

Network	Alpha (α)	AUC	Accuracy	Bonafide Accuracy	Spoofer Accuracy	Placement	d'	FNR @ FPR = 1%	GLS20 ^U Accuracy	VBN ^U Accuracy	RFastPro ^U Accuracy	Wood Glue ^K Accuracy	Body Double ^K Accuracy
ResNet	0.9	0.908 \pm 0.009	0.819 \pm 0.002	0.927 \pm 0.009	0.703 \pm 0.006	6	1.881 \pm 0.074	0.595 \pm 0.024	0.591 \pm 0.010	0.823 \pm 0.012	0.643 \pm 0.016	0.779 \pm 0.027	0.788 \pm 0.008
DenseNet		0.931 \pm 0.013	0.838 \pm 0.022	0.949 \pm 0.013	0.717 \pm 0.050	5-7	2.111 \pm 0.145	0.511 \pm 0.046	0.600 \pm 0.060	0.837 \pm 0.043	0.655 \pm 0.056	0.775 \pm 0.068	0.829 \pm 0.015
Inception		0.959 \pm 0.002	0.879 \pm 0.006	0.966 \pm 0.002	0.786 \pm 0.012	4-5	2.462 \pm 0.036	0.379 \pm 0.039	0.701 \pm 0.024	0.870 \pm 0.004	0.733 \pm 0.014	0.865 \pm 0.013	0.846 \pm 0.015
ResNet	0.7	0.921 \pm 0.017	0.838 \pm 0.022	0.926 \pm 0.016	0.743 \pm 0.037	5-7	2.005 \pm 0.159	0.556 \pm 0.095	0.618 \pm 0.039	0.883 \pm 0.025	0.663 \pm 0.045	0.854 \pm 0.047	0.826 \pm 0.032
DenseNet		0.925 \pm 0.006	0.833 \pm 0.003	0.946 \pm 0.007	0.712 \pm 0.014	5	2.038 \pm 0.060	0.553 \pm 0.013	0.590 \pm 0.027	0.839 \pm 0.019	0.638 \pm 0.018	0.821 \pm 0.028	0.797 \pm 0.011
Inception		0.953 \pm 0.008	0.865 \pm 0.013	0.957 \pm 0.007	0.766 \pm 0.022	4-5	2.377 \pm 0.116	0.424 \pm 0.029	0.668 \pm 0.021	0.863 \pm 0.040	0.713 \pm 0.020	0.856 \pm 0.040	0.830 \pm 0.015
ResNet	0.5	0.927 \pm 0.001	0.840 \pm 0.007	0.940 \pm 0.008	0.731 \pm 0.014	5	2.056 \pm 0.058	0.581 \pm 0.051	0.604 \pm 0.018	0.875 \pm 0.019	0.660 \pm 0.011	0.837 \pm 0.024	0.810 \pm 0.020
DenseNet		0.932 \pm 0.009	0.840 \pm 0.014	0.944 \pm 0.005	0.727 \pm 0.026	5	2.114 \pm 0.101	0.562 \pm 0.034	0.605 \pm 0.039	0.843 \pm 0.039	0.657 \pm 0.011	0.829 \pm 0.048	0.823 \pm 0.015
Inception		0.941 \pm 0.002	0.857 \pm 0.002	0.942 \pm 0.005	0.767 \pm 0.003	5	2.207 \pm 0.024	0.552 \pm 0.021	0.676 \pm 0.009	0.856 \pm 0.020	0.718 \pm 0.023	0.851 \pm 0.040	0.823 \pm 0.010
ResNet	0.3	0.892 \pm 0.011	0.811 \pm 0.011	0.911 \pm 0.011	0.704 \pm 0.015	5-7	1.754 \pm 0.085	0.705 \pm 0.052	0.559 \pm 0.025	0.856 \pm 0.016	0.626 \pm 0.029	0.851 \pm 0.018	0.773 \pm 0.010
DenseNet		0.911 \pm 0.014	0.823 \pm 0.010	0.939 \pm 0.014	0.699 \pm 0.006	5-7	1.912 \pm 0.121	0.622 \pm 0.035	0.549 \pm 0.010	0.856 \pm 0.005	0.613 \pm 0.007	0.870 \pm 0.013	0.766 \pm 0.007
Inception		0.943 \pm 0.009	0.859 \pm 0.013	0.937 \pm 0.004	0.776 \pm 0.024	4-5	2.246 \pm 0.108	0.549 \pm 0.047	0.666 \pm 0.030	0.881 \pm 0.017	0.711 \pm 0.019	0.881 \pm 0.022	0.853 \pm 0.036
ResNet	0.1	0.854 \pm 0.004	0.780 \pm 0.003	0.848 \pm 0.008	0.708 \pm 0.003	8	1.490 \pm 0.025	0.835 \pm 0.030	0.583 \pm 0.011	0.850 \pm 0.020	0.630 \pm 0.014	0.820 \pm 0.020	0.788 \pm 0.012
DenseNet		0.862 \pm 0.019	0.782 \pm 0.020	0.880 \pm 0.007	0.676 \pm 0.037	7-10	1.545 \pm 0.120	0.763 \pm 0.034	0.509 \pm 0.055	0.883 \pm 0.010	0.555 \pm 0.061	0.899 \pm 0.019	0.734 \pm 0.028
Inception		0.915 \pm 0.010	0.836 \pm 0.012	0.891 \pm 0.005	0.777 \pm 0.025	5-6	1.947 \pm 0.093	0.710 \pm 0.039	0.669 \pm 0.030	0.896 \pm 0.008	0.725 \pm 0.031	0.884 \pm 0.032	0.818 \pm 0.022

Table 6. Results for Scenario S3 using human-annotated AOI saliency. Models trained using CYBORG loss in the limited-data context. Averaged over three runs.

Network	Alpha (α)	AUC	Accuracy	Bonafide Accuracy	Spoofer Accuracy	Placement	d'	FNR @ FPR = 1%	GLS20 ^U Accuracy	VBN ^U Accuracy	RFastPro ^U Accuracy	Wood Glue ^K Accuracy	Body Double ^K Accuracy
ResNet	0.9	0.914 \pm 0.007	0.830 \pm 0.005	0.937 \pm 0.007	0.714 \pm 0.006	5	1.932 \pm 0.061	0.576 \pm 0.025	0.611 \pm 0.011	0.806 \pm 0.022	0.651 \pm 0.020	0.769 \pm 0.015	0.833 \pm 0.007
DenseNet		0.940 \pm 0.001	0.860 \pm 0.010	0.951 \pm 0.010	0.762 \pm 0.031	5	2.198 \pm 0.015	0.466 \pm 0.023	0.678 \pm 0.063	0.850 \pm 0.008	0.708 \pm 0.062	0.805 \pm 0.015	0.851 \pm 0.003
Inception		0.953 \pm 0.004	0.868 \pm 0.006	0.961 \pm 0.005	0.769 \pm 0.016	4-5	2.376 \pm 0.054	0.413 \pm 0.039	0.657 \pm 0.043	0.866 \pm 0.032	0.711 \pm 0.050	0.855 \pm 0.048	0.858 \pm 0.016
ResNet	0.7	0.929 \pm 0.009	0.845 \pm 0.014	0.933 \pm 0.026	0.750 \pm 0.021	5	2.080 \pm 0.097	0.582 \pm 0.065	0.652 \pm 0.024	0.853 \pm 0.031	0.700 \pm 0.023	0.796 \pm 0.061	0.839 \pm 0.014
DenseNet		0.937 \pm 0.005	0.853 \pm 0.011	0.941 \pm 0.011	0.759 \pm 0.029	5	2.169 \pm 0.055	0.551 \pm 0.051	0.661 \pm 0.027	0.853 \pm 0.058	0.708 \pm 0.029	0.831 \pm 0.079	0.832 \pm 0.011
Inception		0.948 \pm 0.005	0.860 \pm 0.005	0.952 \pm 0.002	0.761 \pm 0.012	5	2.296 \pm 0.060	0.472 \pm 0.030	0.668 \pm 0.024	0.850 \pm 0.006	0.732 \pm 0.024	0.795 \pm 0.017	0.831 \pm 0.007
ResNet	0.5												

Network	Alpha (α)	AUC	Accuracy	Bonafide Accuracy	Spoof Accuracy	Placement	d^*	FNR @ FPR = 1%	GLS20 ^U Accuracy	VBN ^U Accuracy	RFastPro ^U Accuracy	Wood Glue ^K Accuracy	Body Double ^K Accuracy
ResNet DenseNet Inception	0.9	0.924 \pm 0.014	0.835 \pm 0.017	0.925 \pm 0.008	0.738 \pm 0.032	5-7 5 4-5	2.031 \pm 0.132	0.593 \pm 0.040	0.642 \pm 0.050	0.827 \pm 0.032	0.684 \pm 0.056	0.808 \pm 0.045	0.821 \pm 0.023
		0.942 \pm 0.012	0.861 \pm 0.008	0.948 \pm 0.009	0.768 \pm 0.011		2.236 \pm 0.148	0.468 \pm 0.050	0.689 \pm 0.011	0.846 \pm 0.021	0.723 \pm 0.015	0.824 \pm 0.032	0.833 \pm 0.016
		0.955 \pm 0.002	0.875 \pm 0.003	0.965 \pm 0.002	0.777 \pm 0.007		2.396 \pm 0.028	0.387 \pm 0.011	0.696 \pm 0.019	0.834 \pm 0.036	0.734 \pm 0.015	0.851 \pm 0.039	0.844 \pm 0.020
ResNet DenseNet Inception	0.7	0.925 \pm 0.003	0.847 \pm 0.007	0.923 \pm 0.006	0.765 \pm 0.012	5 5-6 4	2.038 \pm 0.033	0.567 \pm 0.034	0.650 \pm 0.027	0.885 \pm 0.009	0.701 \pm 0.019	0.859 \pm 0.005	0.844 \pm 0.012
		0.922 \pm 0.005	0.828 \pm 0.004	0.934 \pm 0.012	0.713 \pm 0.021		2.007 \pm 0.046	0.624 \pm 0.036	0.627 \pm 0.061	0.754 \pm 0.026	0.671 \pm 0.055	0.770 \pm 0.036	0.813 \pm 0.019
		0.961 \pm 0.004	0.885 \pm 0.004	0.952 \pm 0.006	0.812 \pm 0.014		2.490 \pm 0.067	0.386 \pm 0.041	0.752 \pm 0.019	0.867 \pm 0.013	0.787 \pm 0.021	0.844 \pm 0.016	0.859 \pm 0.011
ResNet DenseNet Inception	0.5	0.924 \pm 0.014	0.853 \pm 0.011	0.928 \pm 0.012	0.771 \pm 0.035	5 5 4	2.031 \pm 0.137	0.479 \pm 0.010	0.684 \pm 0.057	0.857 \pm 0.007	0.721 \pm 0.061	0.837 \pm 0.012	0.843 \pm 0.026
		0.926 \pm 0.007	0.843 \pm 0.009	0.926 \pm 0.013	0.753 \pm 0.004		2.050 \pm 0.075	0.546 \pm 0.050	0.670 \pm 0.017	0.818 \pm 0.033	0.708 \pm 0.015	0.817 \pm 0.034	0.828 \pm 0.016
		0.959 \pm 0.002	0.880 \pm 0.002	0.950 \pm 0.009	0.806 \pm 0.011		2.455 \pm 0.034	0.416 \pm 0.028	0.712 \pm 0.019	0.891 \pm 0.012	0.749 \pm 0.009	0.894 \pm 0.034	0.878 \pm 0.006
ResNet DenseNet Inception	0.3	0.911 \pm 0.005	0.837 \pm 0.005	0.905 \pm 0.013	0.764 \pm 0.009	5 5 5	1.907 \pm 0.046	0.622 \pm 0.011	0.653 \pm 0.038	0.881 \pm 0.024	0.690 \pm 0.029	0.878 \pm 0.024	0.838 \pm 0.016
		0.922 \pm 0.006	0.844 \pm 0.006	0.928 \pm 0.008	0.753 \pm 0.014		2.004 \pm 0.060	0.575 \pm 0.020	0.657 \pm 0.014	0.831 \pm 0.021	0.704 \pm 0.017	0.862 \pm 0.019	0.802 \pm 0.008
		0.944 \pm 0.001	0.864 \pm 0.005	0.945 \pm 0.005	0.777 \pm 0.013		2.249 \pm 0.018	0.520 \pm 0.022	0.681 \pm 0.020	0.868 \pm 0.012	0.720 \pm 0.026	0.855 \pm 0.028	0.858 \pm 0.011
ResNet DenseNet Inception	0.1	0.878 \pm 0.003	0.809 \pm 0.004	0.857 \pm 0.009	0.756 \pm 0.019	7 5-7 5	1.646 \pm 0.021	0.764 \pm 0.016	0.633 \pm 0.029	0.859 \pm 0.010	0.680 \pm 0.033	0.893 \pm 0.015	0.843 \pm 0.013
		0.896 \pm 0.009	0.823 \pm 0.010	0.891 \pm 0.023	0.750 \pm 0.027		1.784 \pm 0.070	0.694 \pm 0.017	0.651 \pm 0.034	0.830 \pm 0.019	0.702 \pm 0.031	0.890 \pm 0.021	0.777 \pm 0.027
		0.932 \pm 0.001	0.852 \pm 0.006	0.907 \pm 0.001	0.794 \pm 0.012		2.106 \pm 0.014	0.631 \pm 0.023	0.716 \pm 0.013	0.850 \pm 0.017	0.758 \pm 0.007	0.860 \pm 0.029	0.853 \pm 0.003

Table 8. Results for Scenario S3 using minutiae-based FOI saliency. Models trained using CYBORG loss in the limited-data context. Averaged over three runs.

Network	Alpha (α)	AUC	Accuracy	Bonafide Accuracy	Spoof Accuracy	Placement	d^*	FNR @ FPR = 1%	GLS20 ^U Accuracy	VBN ^U Accuracy	RFastPro ^U Accuracy	Wood Glue ^K Accuracy	Body Double ^K Accuracy
ResNet DenseNet Inception	0.9	0.930 \pm 0.014	0.853 \pm 0.022	0.927 \pm 0.006	0.774 \pm 0.048	5-6 5-7 4-5	2.097 \pm 0.141	0.520 \pm 0.047	0.687 \pm 0.053	0.860 \pm 0.048	0.731 \pm 0.054	0.839 \pm 0.065	0.834 \pm 0.029
		0.933 \pm 0.005	0.839 \pm 0.023	0.946 \pm 0.010	0.724 \pm 0.057		2.120 \pm 0.053	0.530 \pm 0.018	0.632 \pm 0.068	0.794 \pm 0.064	0.678 \pm 0.069	0.783 \pm 0.062	0.812 \pm 0.031
		0.956 \pm 0.007	0.881 \pm 0.013	0.957 \pm 0.001	0.800 \pm 0.027		2.427 \pm 0.108	0.416 \pm 0.102	0.705 \pm 0.055	0.893 \pm 0.033	0.746 \pm 0.053	0.885 \pm 0.044	0.866 \pm 0.014
ResNet DenseNet Inception	0.7	0.918 \pm 0.003	0.835 \pm 0.011	0.922 \pm 0.014	0.740 \pm 0.020	5-6 5 5	1.968 \pm 0.032	0.593 \pm 0.061	0.645 \pm 0.047	0.830 \pm 0.019	0.681 \pm 0.049	0.806 \pm 0.030	0.831 \pm 0.006
		0.930 \pm 0.006	0.846 \pm 0.005	0.939 \pm 0.006	0.745 \pm 0.013		2.088 \pm 0.064	0.557 \pm 0.051	0.655 \pm 0.025	0.814 \pm 0.044	0.716 \pm 0.017	0.792 \pm 0.037	0.820 \pm 0.022
		0.943 \pm 0.002	0.860 \pm 0.005	0.951 \pm 0.003	0.761 \pm 0.013		2.234 \pm 0.022	0.485 \pm 0.046	0.671 \pm 0.014	0.853 \pm 0.024	0.694 \pm 0.015	0.852 \pm 0.052	0.835 \pm 0.023
ResNet DenseNet Inception	0.5	0.923 \pm 0.005	0.842 \pm 0.010	0.918 \pm 0.010	0.759 \pm 0.016	5 5-6 4-5	2.022 \pm 0.052	0.550 \pm 0.042	0.648 \pm 0.024	0.855 \pm 0.018	0.703 \pm 0.018	0.849 \pm 0.025	0.847 \pm 0.014
		0.914 \pm 0.007	0.830 \pm 0.011	0.922 \pm 0.009	0.731 \pm 0.032		1.933 \pm 0.066	0.658 \pm 0.043	0.645 \pm 0.064	0.801 \pm 0.010	0.686 \pm 0.064	0.816 \pm 0.020	0.789 \pm 0.020
		0.953 \pm 0.006	0.871 \pm 0.006	0.949 \pm 0.009	0.786 \pm 0.007		2.374 \pm 0.088	0.447 \pm 0.016	0.699 \pm 0.006	0.860 \pm 0.025	0.751 \pm 0.004	0.861 \pm 0.019	0.839 \pm 0.008
ResNet DenseNet Inception	0.3	0.913 \pm 0.015	0.838 \pm 0.014	0.902 \pm 0.016	0.769 \pm 0.015	5-6 5 5	1.933 \pm 0.126	0.600 \pm 0.022	0.654 \pm 0.022	0.883 \pm 0.017	0.699 \pm 0.019	0.890 \pm 0.010	0.839 \pm 0.009
		0.909 \pm 0.008	0.838 \pm 0.004	0.905 \pm 0.016	0.767 \pm 0.010		1.893 \pm 0.071	0.681 \pm 0.056	0.670 \pm 0.006	0.849 \pm 0.021	0.721 \pm 0.015	0.883 \pm 0.022	0.805 \pm 0.011
		0.940 \pm 0.007	0.861 \pm 0.010	0.934 \pm 0.002	0.783 \pm 0.018		2.198 \pm 0.081	0.521 \pm 0.043	0.693 \pm 0.023	0.873 \pm 0.030	0.725 \pm 0.027	0.866 \pm 0.010	0.853 \pm 0.025
ResNet DenseNet Inception	0.1	0.886 \pm 0.007	0.815 \pm 0.008	0.858 \pm 0.012	0.768 \pm 0.016	5-7 5-7 5	1.704 \pm 0.054	0.759 \pm 0.009	0.656 \pm 0.017	0.855 \pm 0.040	0.710 \pm 0.011	0.872 \pm 0.040	0.852 \pm 0.012
		0.893 \pm 0.008	0.819 \pm 0.006	0.895 \pm 0.014	0.736 \pm 0.010		1.756 \pm 0.064	0.745 \pm 0.053	0.625 \pm 0.011	0.824 \pm 0.010	0.679 \pm 0.020	0.886 \pm 0.005	0.780 \pm 0.010
		0.924 \pm 0.005	0.846 \pm 0.004	0.901 \pm 0.011	0.787 \pm 0.010		2.026 \pm 0.051	0.665 \pm 0.046	0.684 \pm 0.025	0.873 \pm 0.021	0.735 \pm 0.021	0.894 \pm 0.014	0.845 \pm 0.009

Table 9. Results for Scenario S3 using minutiae-based AOI saliency. Models trained using CYBORG loss in the limited-data context. Averaged over three runs.

Network	Alpha (α)	AUC	Accuracy	Bonafide Accuracy	Spoof Accuracy	Placement	d^*	FNR @ FPR = 1%	GLS20 ^U Accuracy	VBN ^U Accuracy	RFastPro ^U Accuracy	Wood Glue ^K Accuracy	Body Double ^K Accuracy
ResNet DenseNet Inception	0.9	0.912 \pm 0.006	0.828 \pm 0.012	0.925 \pm 0.009	0.724 \pm 0.015	5-6 5 4-5	1.912 \pm 0.054	0.576 \pm 0.049	0.606 \pm 0.032	0.839 \pm 0.027	0.654 \pm 0.026	0.820 \pm 0.028	0.816 \pm 0.023
		0.929 \pm 0.004	0.841 \pm 0.006	0.945 \pm 0.014	0.728 \pm 0.020		2.079 \pm 0.042	0.509 \pm 0.024	0.628 \pm 0.053	0.790 \pm 0.061	0.688 \pm 0.051	0.765 \pm 0.076	0.845 \pm 0.009
		0.951 \pm 0.003	0.867 \pm 0.001	0.961 \pm 0.008	0.765 \pm 0.009		2.338 \pm 0.046	0.430 \pm 0.037	0.665 \pm 0.051	0.857 \pm 0.037	0.715 \pm 0.037	0.849 \pm 0.042	0.835 \pm 0.016
ResNet DenseNet Inception	0.7	0.909 \pm 0.016	0.825 \pm 0.022	0.929 \pm 0.003	0.712 \pm 0.043	5-7 5-6 4-5	1.898 \pm 0.135	0.576 \pm 0.044</td					

Network	Alpha (α)	AUC	Accuracy	Bonafide Accuracy	Spoof Accuracy	Placement	d^*	FNR @ FPR = 1%	GLS20 ^U Accuracy	VBN ^U Accuracy	RFastPro ^U Accuracy	Wood Glue ^K Accuracy	Body Double ^K Accuracy
ResNet DenseNet Inception	0.9	0.931 \pm 0.002	0.836 \pm 0.010	0.941 \pm 0.004	0.722 \pm 0.019	5-6 5 4-5	2.093 \pm 0.017	0.582 \pm 0.016	0.603 \pm 0.024	0.862 \pm 0.018	0.642 \pm 0.020	0.807 \pm 0.030	0.822 \pm 0.018
		0.931 \pm 0.006	0.846 \pm 0.013	0.940 \pm 0.009	0.745 \pm 0.036		2.102 \pm 0.067	0.529 \pm 0.024	0.650 \pm 0.044	0.834 \pm 0.040	0.696 \pm 0.044	0.808 \pm 0.054	0.828 \pm 0.010
		0.955 \pm 0.004	0.873 \pm 0.005	0.957 \pm 0.010	0.782 \pm 0.009		2.404 \pm 0.068	0.441 \pm 0.078	0.698 \pm 0.007	0.866 \pm 0.022	0.740 \pm 0.018	0.820 \pm 0.015	0.862 \pm 0.005
ResNet DenseNet Inception	0.7	0.911 \pm 0.018	0.831 \pm 0.014	0.921 \pm 0.016	0.734 \pm 0.019	5-7 5 4-5	1.920 \pm 0.155	0.614 \pm 0.062	0.596 \pm 0.041	0.900 \pm 0.002	0.638 \pm 0.038	0.884 \pm 0.020	0.809 \pm 0.007
		0.936 \pm 0.004	0.858 \pm 0.002	0.932 \pm 0.003	0.777 \pm 0.006		2.156 \pm 0.044	0.540 \pm 0.022	0.686 \pm 0.015	0.886 \pm 0.014	0.726 \pm 0.014	0.882 \pm 0.021	0.804 \pm 0.010
		0.951 \pm 0.005	0.874 \pm 0.007	0.948 \pm 0.004	0.795 \pm 0.019		2.350 \pm 0.077	0.469 \pm 0.029	0.718 \pm 0.022	0.877 \pm 0.023	0.756 \pm 0.021	0.861 \pm 0.028	0.838 \pm 0.022
ResNet DenseNet Inception	0.5	0.907 \pm 0.014	0.830 \pm 0.018	0.910 \pm 0.023	0.743 \pm 0.023	5-7 5-7 4-5	1.872 \pm 0.116	0.678 \pm 0.092	0.607 \pm 0.038	0.905 \pm 0.002	0.650 \pm 0.035	0.916 \pm 0.006	0.795 \pm 0.028
		0.911 \pm 0.009	0.828 \pm 0.012	0.902 \pm 0.014	0.748 \pm 0.015		1.903 \pm 0.074	0.662 \pm 0.036	0.616 \pm 0.021	0.905 \pm 0.005	0.669 \pm 0.015	0.916 \pm 0.015	0.785 \pm 0.019
		0.953 \pm 0.007	0.876 \pm 0.011	0.953 \pm 0.014	0.793 \pm 0.023		2.378 \pm 0.097	0.424 \pm 0.051	0.699 \pm 0.030	0.898 \pm 0.024	0.742 \pm 0.020	0.891 \pm 0.023	0.829 \pm 0.021
ResNet DenseNet Inception	0.3	0.882 \pm 0.002	0.810 \pm 0.006	0.889 \pm 0.006	0.725 \pm 0.006	6-7 5-6 5	1.674 \pm 0.016	0.765 \pm 0.053	0.586 \pm 0.010	0.889 \pm 0.003	0.641 \pm 0.009	0.914 \pm 0.006	0.750 \pm 0.007
		0.902 \pm 0.003	0.820 \pm 0.005	0.911 \pm 0.003	0.722 \pm 0.007		1.831 \pm 0.028	0.703 \pm 0.021	0.586 \pm 0.005	0.890 \pm 0.016	0.647 \pm 0.009	0.899 \pm 0.017	0.740 \pm 0.020
		0.932 \pm 0.000	0.852 \pm 0.006	0.928 \pm 0.010	0.770 \pm 0.023		2.111 \pm 0.003	0.635 \pm 0.010	0.653 \pm 0.032	0.898 \pm 0.020	0.711 \pm 0.028	0.903 \pm 0.021	0.803 \pm 0.017
ResNet DenseNet Inception	0.1	0.860 \pm 0.001	0.786 \pm 0.001	0.853 \pm 0.004	0.713 \pm 0.005	7 7-8 5-7	1.531 \pm 0.009	0.873 \pm 0.026	0.577 \pm 0.009	0.884 \pm 0.004	0.623 \pm 0.003	0.905 \pm 0.007	0.736 \pm 0.007
		0.872 \pm 0.006	0.783 \pm 0.005	0.869 \pm 0.006	0.691 \pm 0.009		1.605 \pm 0.040	0.801 \pm 0.021	0.532 \pm 0.015	0.897 \pm 0.005	0.594 \pm 0.019	0.910 \pm 0.015	0.705 \pm 0.011
		0.899 \pm 0.008	0.817 \pm 0.007	0.876 \pm 0.011	0.754 \pm 0.011		1.806 \pm 0.062	0.751 \pm 0.042	0.631 \pm 0.012	0.890 \pm 0.008	0.705 \pm 0.015	0.889 \pm 0.010	0.776 \pm 0.020

Table 11. Results for Scenario S3 using low-quality map saliency. Models trained using CYBORG loss in the limited-data context. Averaged over three runs.

D. Scenario S4, Full Results

Network	Saliency	AUC	Accuracy	Bonafide Accuracy	Spoof Accuracy	Placement	d^*	FNR @ FPR = 1%	GLS20 ^U Accuracy	VBN ^U Accuracy	RFastPro ^U Accuracy	Wood Glue ^K Accuracy	Body Double ^K Accuracy
ResNet DenseNet Inception	None	0.869 \pm 0.015	0.786 \pm 0.011	0.876 \pm 0.017	0.689 \pm 0.020	7-8 7-12 6-9	1.593 \pm 0.100	0.769 \pm 0.037	0.668 \pm 0.006	0.707 \pm 0.043	0.709 \pm 0.007	0.623 \pm 0.048	0.729 \pm 0.055
		0.846 \pm 0.027	0.762 \pm 0.023	0.837 \pm 0.004	0.681 \pm 0.049		1.452 \pm 0.158	0.785 \pm 0.008	0.660 \pm 0.028	0.712 \pm 0.109	0.705 \pm 0.037	0.598 \pm 0.095	0.721 \pm 0.019
		0.878 \pm 0.013	0.794 \pm 0.018	0.869 \pm 0.019	0.714 \pm 0.057		1.652 \pm 0.094	0.741 \pm 0.030	0.713 \pm 0.039	0.691 \pm 0.094	0.758 \pm 0.042	0.588 \pm 0.123	0.773 \pm 0.031
ResNet DenseNet Inception	Human FOI	0.882 \pm 0.005	0.798 \pm 0.007	0.884 \pm 0.009	0.704 \pm 0.018	7 5 5	1.677 \pm 0.033	0.768 \pm 0.047	0.550 \pm 0.038	0.881 \pm 0.015	0.619 \pm 0.016	0.852 \pm 0.020	0.779 \pm 0.018
		0.922 \pm 0.006	0.838 \pm 0.011	0.923 \pm 0.008	0.747 \pm 0.030		2.010 \pm 0.061	0.621 \pm 0.019	0.661 \pm 0.005	0.842 \pm 0.060	0.704 \pm 0.020	0.784 \pm 0.080	0.823 \pm 0.017
		0.935 \pm 0.006	0.855 \pm 0.005	0.924 \pm 0.004	0.782 \pm 0.013		2.144 \pm 0.066	0.501 \pm 0.009	0.700 \pm 0.030	0.866 \pm 0.015	0.745 \pm 0.033	0.844 \pm 0.046	0.830 \pm 0.025
ResNet DenseNet Inception	Human AOI	0.916 \pm 0.012	0.832 \pm 0.011	0.930 \pm 0.008	0.727 \pm 0.029	5-6 4-5 5	1.959 \pm 0.111	0.586 \pm 0.050	0.593 \pm 0.051	0.847 \pm 0.004	0.653 \pm 0.053	0.848 \pm 0.002	0.823 \pm 0.025
		0.939 \pm 0.008	0.863 \pm 0.012	0.952 \pm 0.005	0.767 \pm 0.020		2.191 \pm 0.089	0.471 \pm 0.059	0.6894 \pm 0.040	0.830 \pm 0.017	0.720 \pm 0.036	0.831 \pm 0.023	0.840 \pm 0.030
		0.947 \pm 0.008	0.866 \pm 0.005	0.960 \pm 0.009	0.764 \pm 0.011		2.290 \pm 0.096	0.422 \pm 0.017	0.645 \pm 0.013	0.864 \pm 0.012	0.699 \pm 0.020	0.872 \pm 0.016	0.857 \pm 0.013
ResNet DenseNet Inception	Human BOI	0.927 \pm 0.010	0.846 \pm 0.010	0.928 \pm 0.018	0.758 \pm 0.024	5 5 4-5	2.067 \pm 0.107	0.530 \pm 0.017	0.657 \pm 0.040	0.871 \pm 0.010	0.693 \pm 0.045	0.865 \pm 0.023	0.814 \pm 0.026
		0.944 \pm 0.001	0.857 \pm 0.006	0.954 \pm 0.004	0.753 \pm 0.016		2.251 \pm 0.011	0.477 \pm 0.022	0.666 \pm 0.032	0.838 \pm 0.009	0.707 \pm 0.035	0.804 \pm 0.035	0.829 \pm 0.014
		0.953 \pm 0.004	0.873 \pm 0.006	0.958 \pm 0.007	0.781 \pm 0.015		2.374 \pm 0.055	0.410 \pm 0.041	0.708 \pm 0.020	0.840 \pm 0.014	0.753 \pm 0.008	0.824 \pm 0.026	0.842 \pm 0.035
ResNet DenseNet Inception	Minutiae FOI	0.883 \pm 0.024	0.802 \pm 0.029	0.831 \pm 0.037	0.771 \pm 0.021	5-10 5-7 5	1.698 \pm 0.175	0.734 \pm 0.014	0.693 \pm 0.020	0.881 \pm 0.024	0.732 \pm 0.012	0.866 \pm 0.035	0.772 \pm 0.047
		0.896 \pm 0.027	0.820 \pm 0.022	0.843 \pm 0.026	0.795 \pm 0.018		1.797 \pm 0.198	0.728 \pm 0.099	0.704 \pm 0.025	0.894 \pm 0.017	0.737 \pm 0.021	0.914 \pm 0.030	0.826 \pm 0.004
		0.933 \pm 0.005	0.857 \pm 0.006	0.872 \pm 0.017	0.841 \pm 0.032		2.117 \pm 0.053	0.611 \pm 0.039	0.787 \pm 0.054	0.892 \pm 0.017	0.824 \pm 0.040	0.904 \pm 0.027	0.847 \pm 0.018
ResNet DenseNet Inception	Minutiae AOI	0.903 \pm 0.006	0.821 \pm 0.009	0.874 \pm 0.018	0.765 \pm 0.023	5-7 5 4-5	1.837 \pm 0.052	0.664 \pm 0.035	0.670 \pm 0.039	0.862 \pm 0.024	0.707 \pm 0.043	0.860 \pm 0.020	0.824 \pm 0.015
		0.932 \pm 0.003	0.856 \pm 0.007	0.906 \pm 0.004	0.801 \pm 0.011		2.109 \pm 0.028	0.514 \pm 0.019	0.707 \pm 0.013	0.895 \pm 0.016	0.749 \pm 0.020	0.904 \pm 0.013	0.845 \pm 0.033
		0.942 \pm 0.006	0.868 \pm 0.008	0.907 \pm 0.008	0.825 \pm 0.020		2.221 \pm 0.070	0.519 \pm 0.019	0.762 \pm 0.041	0.864 \pm 0.024	0.800 \pm 0.036	0.886 \pm 0.020	0.866 \pm 0.002
ResNet DenseNet Inception	Minutiae BOI	0.917 \pm 0.016	0.837 \pm 0.015	0.934 \pm 0.002	0.731 \pm 0.030	5-6 5 5	1.971 \pm 0.154	0.545 \pm 0.026	0.631 \pm 0.037	0.835 \pm 0.026	0.681 \pm 0.034	0.791 \pm 0.044	0.812 \pm 0.020
		0.921 \pm 0.009	0.839 \pm 0.005	0.943 \pm 0.008	0.726 \pm 0.015		2.002 \pm 0.082	0.510 \pm 0.019	0.627 \pm 0.053	0.819 \pm 0.052	0.674 \pm 0.050	0.768 \pm 0.054	0.832 \pm 0.039
		0.950 \pm 0.006	0.866 \pm 0.005	0.953 \pm 0.007	0.772 \pm 0.004		2.325 \pm 0.077	0.448 \pm 0.017	0.696 \pm 0.018	0.856 $\pm</math$			

E. Scenario S5, Full Results

Network	Alpha (α)	AUC	Accuracy	Bonafide Accuracy	Spoofer Accuracy	Placement	d^*	FNR @ FPR = 1%	GLS20 ^U Accuracy	VBN ^U Accuracy	RFastPro ^U Accuracy	Wood Glue ^K Accuracy	Body Double ^K Accuracy
ResNet	0.9	0.988 \pm 0.001	0.900 \pm 0.007	0.996 \pm 0.001	0.795 \pm 0.016	4	3.199 \pm 0.065	0.141 \pm 0.008	0.704 \pm 0.026	0.897 \pm 0.002	0.727 \pm 0.024	0.886 \pm 0.016	0.864 \pm 0.005
DenseNet		0.982 \pm 0.001	0.894 \pm 0.007	0.991 \pm 0.003	0.790 \pm 0.017	4	2.978 \pm 0.020	0.201 \pm 0.017	0.685 \pm 0.026	0.909 \pm 0.007	0.716 \pm 0.022	0.919 \pm 0.017	0.838 \pm 0.016
Inception		0.991 \pm 0.001	0.911 \pm 0.016	0.995 \pm 0.003	0.822 \pm 0.037	2-4	3.528 \pm 0.075	0.132 \pm 0.008	0.738 \pm 0.055	0.905 \pm 0.014	0.751 \pm 0.061	0.912 \pm 0.009	0.898 \pm 0.028
ResNet	0.7	0.982 \pm 0.001	0.891 \pm 0.007	0.994 \pm 0.001	0.780 \pm 0.015	4	2.965 \pm 0.045	0.179 \pm 0.005	0.690 \pm 0.015	0.875 \pm 0.019	0.715 \pm 0.015	0.890 \pm 0.018	0.831 \pm 0.015
DenseNet		0.976 \pm 0.001	0.891 \pm 0.008	0.979 \pm 0.001	0.797 \pm 0.017	4	2.786 \pm 0.020	0.308 \pm 0.017	0.700 \pm 0.025	0.922 \pm 0.002	0.716 \pm 0.034	0.934 \pm 0.009	0.838 \pm 0.016
Inception		0.986 \pm 0.002	0.906 \pm 0.001	0.992 \pm 0.002	0.815 \pm 0.005	4	3.124 \pm 0.070	0.169 \pm 0.016	0.719 \pm 0.011	0.929 \pm 0.012	0.742 \pm 0.019	0.919 \pm 0.018	0.873 \pm 0.002
ResNet	0.5	0.965 \pm 0.007	0.868 \pm 0.005	0.987 \pm 0.003	0.739 \pm 0.008	4-5	2.569 \pm 0.137	0.291 \pm 0.033	0.621 \pm 0.016	0.879 \pm 0.005	0.655 \pm 0.018	0.884 \pm 0.008	0.794 \pm 0.012
DenseNet		0.949 \pm 0.008	0.844 \pm 0.004	0.973 \pm 0.006	0.704 \pm 0.011	5	2.323 \pm 0.109	0.407 \pm 0.036	0.563 \pm 0.011	0.883 \pm 0.018	0.588 \pm 0.004	0.907 \pm 0.018	0.757 \pm 0.018
Inception		0.982 \pm 0.001	0.894 \pm 0.008	0.991 \pm 0.002	0.789 \pm 0.018	4	2.972 \pm 0.040	0.201 \pm 0.008	0.680 \pm 0.015	0.922 \pm 0.020	0.709 \pm 0.017	0.924 \pm 0.014	0.836 \pm 0.027
ResNet	0.3	0.951 \pm 0.005	0.843 \pm 0.006	0.979 \pm 0.004	0.697 \pm 0.012	5	2.349 \pm 0.072	0.383 \pm 0.023	0.574 \pm 0.012	0.844 \pm 0.017	0.605 \pm 0.020	0.853 \pm 0.014	0.753 \pm 0.013
DenseNet		0.956 \pm 0.010	0.850 \pm 0.014	0.969 \pm 0.004	0.722 \pm 0.025	5	2.430 \pm 0.152	0.439 \pm 0.046	0.589 \pm 0.026	0.900 \pm 0.015	0.614 \pm 0.025	0.911 \pm 0.035	0.763 \pm 0.023
Inception		0.983 \pm 0.003	0.898 \pm 0.007	0.993 \pm 0.001	0.796 \pm 0.014	4	3.021 \pm 0.092	0.177 \pm 0.025	0.692 \pm 0.029	0.919 \pm 0.006	0.723 \pm 0.027	0.920 \pm 0.005	0.844 \pm 0.001
ResNet	0.1	0.937 \pm 0.001	0.815 \pm 0.004	0.972 \pm 0.004	0.645 \pm 0.013	6-7	2.161 \pm 0.015	0.383 \pm 0.023	0.574 \pm 0.012	0.844 \pm 0.017	0.605 \pm 0.020	0.822 \pm 0.009	0.714 \pm 0.007
DenseNet		0.946 \pm 0.007	0.847 \pm 0.004	0.955 \pm 0.008	0.732 \pm 0.007	5	2.276 \pm 0.087	0.481 \pm 0.043	0.614 \pm 0.009	0.880 \pm 0.008	0.645 \pm 0.006	0.898 \pm 0.009	0.763 \pm 0.012
Inception		0.975 \pm 0.003	0.882 \pm 0.002	0.989 \pm 0.003	0.767 \pm 0.007	4	2.779 \pm 0.077	0.236 \pm 0.015	0.647 \pm 0.012	0.902 \pm 0.004	0.693 \pm 0.016	0.910 \pm 0.008	0.817 \pm 0.007

Table 13. Results for Scenario S5 using autoencoder-generated FOI saliency. Models trained using CYBORG in the large-data-availability context. Averaged over three runs.

Network	Alpha (α)	AUC	Accuracy	Bonafide Accuracy	Spoofer Accuracy	Placement	d^*	FNR @ FPR = 1%	GLS20 ^U Accuracy	VBN ^U Accuracy	RFastPro ^U Accuracy	Wood Glue ^K Accuracy	Body Double ^K Accuracy
ResNet	0.9	0.987 \pm 0.000	0.904 \pm 0.008	0.995 \pm 0.001	0.806 \pm 0.017	3-4	3.141 \pm 0.018	0.154 \pm 0.018	0.719 \pm 0.011	0.904 \pm 0.018	0.747 \pm 0.015	0.904 \pm 0.020	0.854 \pm 0.027
DenseNet		0.985 \pm 0.003	0.899 \pm 0.015	0.993 \pm 0.002	0.798 \pm 0.033	4	3.092 \pm 0.122	0.179 \pm 0.019	0.694 \pm 0.037	0.909 \pm 0.021	0.727 \pm 0.043	0.915 \pm 0.022	0.859 \pm 0.034
Inception		0.990 \pm 0.001	0.916 \pm 0.011	0.994 \pm 0.001	0.831 \pm 0.024	2-4	3.317 \pm 0.084	0.131 \pm 0.008	0.742 \pm 0.033	0.931 \pm 0.012	0.765 \pm 0.029	0.938 \pm 0.015	0.881 \pm 0.030
ResNet	0.7	0.986 \pm 0.001	0.899 \pm 0.005	0.995 \pm 0.001	0.795 \pm 0.009	4	3.090 \pm 0.041	0.166 \pm 0.017	0.709 \pm 0.006	0.906 \pm 0.019	0.728 \pm 0.006	0.899 \pm 0.032	0.838 \pm 0.007
DenseNet		0.966 \pm 0.005	0.868 \pm 0.015	0.976 \pm 0.003	0.752 \pm 0.034	4-5	2.587 \pm 0.100	0.352 \pm 0.023	0.628 \pm 0.041	0.917 \pm 0.013	0.644 \pm 0.048	0.926 \pm 0.024	0.803 \pm 0.035
Inception		0.980 \pm 0.002	0.895 \pm 0.005	0.990 \pm 0.002	0.793 \pm 0.008	4	2.915 \pm 0.056	0.203 \pm 0.021	0.673 \pm 0.021	0.934 \pm 0.006	0.706 \pm 0.026	0.937 \pm 0.019	0.853 \pm 0.008
ResNet	0.5	0.975 \pm 0.002	0.877 \pm 0.003	0.990 \pm 0.001	0.755 \pm 0.006	4-5	2.776 \pm 0.058	0.243 \pm 0.013	0.621 \pm 0.005	0.901 \pm 0.014	0.662 \pm 0.006	0.921 \pm 0.006	0.822 \pm 0.019
DenseNet		0.961 \pm 0.008	0.861 \pm 0.015	0.975 \pm 0.006	0.739 \pm 0.033	4-5	2.510 \pm 0.139	0.375 \pm 0.044	0.577 \pm 0.057	0.926 \pm 0.007	0.608 \pm 0.050	0.950 \pm 0.007	0.828 \pm 0.029
Inception		0.985 \pm 0.003	0.907 \pm 0.008	0.992 \pm 0.002	0.815 \pm 0.018	3-4	3.083 \pm 0.104	0.170 \pm 0.010	0.701 \pm 0.021	0.934 \pm 0.009	0.747 \pm 0.030	0.946 \pm 0.008	0.868 \pm 0.021
ResNet	0.3	0.958 \pm 0.006	0.857 \pm 0.006	0.979 \pm 0.000	0.726 \pm 0.014	5	2.450 \pm 0.096	0.368 \pm 0.003	0.584 \pm 0.018	0.898 \pm 0.005	0.617 \pm 0.020	0.910 \pm 0.008	0.791 \pm 0.019
DenseNet		0.960 \pm 0.009	0.860 \pm 0.009	0.966 \pm 0.010	0.745 \pm 0.018	5	2.490 \pm 0.140	0.413 \pm 0.026	0.603 \pm 0.024	0.912 \pm 0.005	0.638 \pm 0.029	0.936 \pm 0.002	0.803 \pm 0.018
Inception		0.983 \pm 0.001	0.886 \pm 0.001	0.992 \pm 0.003	0.773 \pm 0.004	4	2.993 \pm 0.041	0.215 \pm 0.022	0.657 \pm 0.010	0.911 \pm 0.007	0.701 \pm 0.018	0.907 \pm 0.012	0.817 \pm 0.013
ResNet	0.1	0.947 \pm 0.005	0.844 \pm 0.003	0.964 \pm 0.001	0.715 \pm 0.008	5	2.282 \pm 0.062	0.439 \pm 0.016	0.581 \pm 0.003	0.874 \pm 0.017	0.617 \pm 0.013	0.884 \pm 0.020	0.774 \pm 0.018
DenseNet		0.962 \pm 0.005	0.869 \pm 0.007	0.960 \pm 0.005	0.771 \pm 0.010	4-5	2.520 \pm 0.092	0.408 \pm 0.023	0.645 \pm 0.020	0.921 \pm 0.008	0.688 \pm 0.022	0.931 \pm 0.006	0.814 \pm 0.006
Inception		0.978 \pm 0.002	0.875 \pm 0.004	0.989 \pm 0.001	0.752 \pm 0.008	4-5	2.848 \pm 0.045	0.265 \pm 0.005	0.637 \pm 0.008	0.897 \pm 0.016	0.677 \pm 0.008	0.884 \pm 0.012	0.795 \pm 0.003

Table 14. Results for Scenario S5 using autoencoder-generated AOI saliency. Models trained using CYBORG in the large-data-availability context. Averaged over three runs.

Network	Alpha (α)	AUC	Accuracy	Bonafide Accuracy	Spoofer Accuracy	Placement	d^*	FNR @ FPR = 1%	GLS20 ^U Accuracy	VBN ^U Accuracy	RFastPro ^U Accuracy	Wood Glue ^K Accuracy	Body Double ^K Accuracy
ResNet	0.9	0.989 \pm 0.001	0.911 \pm 0.003	0.996 \pm 0.000	0.819 \pm 0.005	4	3.222 \pm 0.050	0.140 \pm 0.008	0.745 \pm 0.010	0.889 \pm 0.005	0.777 \pm 0.017	0.886 \pm 0.006	0.870 \pm 0.003
DenseNet		0.990 \pm 0.002	0.924 \pm 0.001	0.991 \pm 0.001	0.850 \pm 0.003	3	3.312 \pm 0.115	0.139 \pm 0.007	0.776 \pm 0.014	0.927 \pm 0.021	0.804 \pm 0.016	0.931 \pm 0.022	0.892 \pm 0.008
Inception		0.989 \pm 0.001	0.904 \pm 0.008	0.997 \pm 0.000	0.804 \pm 0.017	4	3.243 \pm 0.055	0.134 \pm 0.011	0.715 \pm 0.022	0.900 \pm 0.018	0.747 \pm 0.014	0.905 \pm 0.013	0.851 \pm 0.030
ResNet	0.7	0.988 \pm 0.001	0.899 \pm 0.006	0.996 \pm 0.001	0.795 \pm 0.013	4	3.174 \pm 0.032	0.147 \pm 0.007	0.721 \pm 0.016	0.873 \pm 0.021	0.740 \pm 0.013	0.867 \pm 0.027	0.854 \pm 0.007
DenseNet		0.974 \pm 0.004	0.885 \pm 0.008	0.977 \pm 0.003	0.786 \pm 0.013	4	2.757 \pm 0.100	0.362 \pm 0.057	0.716 \pm 0.028	0.875 \pm 0.014	0.729 \pm 0.018	0.875 \pm 0.010	0.821 \pm 0.017
Inception		0.987 \pm 0.002	0.913 \pm 0.004	0.991 \pm 0.003	0.830 \pm 0.010	3-4	3.147 \pm 0.088	0.163 \pm 0.022	0.749 \pm 0.014	0.916 \pm 0.004	0.778 \pm 0.017	0.931 \pm 0.011	0.864 \pm 0.007
ResNet	0.5	0.982<											

Network	Alpha (α)	AUC	Accuracy	Bonafide Accuracy	Spoof Accuracy	Placement	d^*	FNR @ FPR = 1%	GLS20 ^U Accuracy	VBN ^U Accuracy	RFastPro ^U Accuracy	Wood Glue ^K Accuracy	Body Double ^K Accuracy
ResNet DenseNet Inception	0.9	0.985 \pm 0.002	0.899 \pm 0.003	0.994 \pm 0.002	0.795 \pm 0.004	4	3.079 \pm 0.089	0.161 \pm 0.013	0.708 \pm 0.011	0.875 \pm 0.031	0.738 \pm 0.014	0.893 \pm 0.016	0.855 \pm 0.006
		0.988 \pm 0.002	0.922 \pm 0.008	0.989 \pm 0.003	0.849 \pm 0.019	2-3	3.179 \pm 0.076	0.153 \pm 0.013	0.774 \pm 0.027	0.893 \pm 0.018	0.807 \pm 0.018	0.937 \pm 0.012	0.903 \pm 0.022
		0.989 \pm 0.002	0.914 \pm 0.001	0.995 \pm 0.000	0.826 \pm 0.001	3-4	3.235 \pm 0.097	0.132 \pm 0.005	0.731 \pm 0.005	0.920 \pm 0.008	0.765 \pm 0.003	0.919 \pm 0.016	0.892 \pm 0.005
ResNet DenseNet Inception	0.7	0.985 \pm 0.002	0.910 \pm 0.003	0.991 \pm 0.003	0.821 \pm 0.004	4	3.086 \pm 0.066	0.166 \pm 0.016	0.752 \pm 0.011	0.890 \pm 0.009	0.774 \pm 0.012	0.891 \pm 0.009	0.873 \pm 0.004
		0.977 \pm 0.006	0.920 \pm 0.011	0.933 \pm 0.013	0.906 \pm 0.009	2-4	2.837 \pm 0.153	0.287 \pm 0.057	0.853 \pm 0.010	0.929 \pm 0.001	0.886 \pm 0.011	0.966 \pm 0.010	0.940 \pm 0.016
		0.987 \pm 0.001	0.920 \pm 0.007	0.988 \pm 0.002	0.847 \pm 0.017	3-4	3.154 \pm 0.022	0.159 \pm 0.003	0.758 \pm 0.029	0.940 \pm 0.015	0.794 \pm 0.031	0.952 \pm 0.018	0.887 \pm 0.021
ResNet DenseNet Inception	0.5	0.960 \pm 0.003	0.887 \pm 0.003	0.949 \pm 0.010	0.820 \pm 0.007	4	2.481 \pm 0.050	0.313 \pm 0.015	0.754 \pm 0.005	0.869 \pm 0.017	0.782 \pm 0.012	0.894 \pm 0.008	0.866 \pm 0.009
		0.951 \pm 0.011	0.877 \pm 0.015	0.893 \pm 0.026	0.861 \pm 0.006	4-5	2.355 \pm 0.155	0.446 \pm 0.042	0.810 \pm 0.002	0.881 \pm 0.019	0.842 \pm 0.004	0.923 \pm 0.009	0.891 \pm 0.005
		0.985 \pm 0.001	0.933 \pm 0.003	0.944 \pm 0.008	0.922 \pm 0.002	2	3.052 \pm 0.021	0.192 \pm 0.012	0.862 \pm 0.002	0.969 \pm 0.002	0.897 \pm 0.007	0.981 \pm 0.001	0.955 \pm 0.001
ResNet DenseNet Inception	0.3	0.915 \pm 0.008	0.830 \pm 0.009	0.878 \pm 0.005	0.777 \pm 0.017	5-6	1.939 \pm 0.068	0.577 \pm 0.024	0.726 \pm 0.018	0.804 \pm 0.024	0.756 \pm 0.021	0.829 \pm 0.020	0.813 \pm 0.015
		0.931 \pm 0.006	0.851 \pm 0.008	0.874 \pm 0.018	0.826 \pm 0.005	5	2.096 \pm 0.067	0.540 \pm 0.040	0.778 \pm 0.012	0.871 \pm 0.009	0.809 \pm 0.007	0.883 \pm 0.001	0.836 \pm 0.004
		0.975 \pm 0.004	0.913 \pm 0.007	0.921 \pm 0.014	0.905 \pm 0.010	3-4	2.776 \pm 0.096	0.302 \pm 0.039	0.848 \pm 0.013	0.952 \pm 0.004	0.880 \pm 0.013	0.971 \pm 0.006	0.929 \pm 0.016
ResNet DenseNet Inception	0.1	0.873 \pm 0.016	0.789 \pm 0.014	0.815 \pm 0.019	0.761 \pm 0.010	7-9	1.616 \pm 0.106	0.904 \pm 0.136	0.705 \pm 0.009	0.797 \pm 0.014	0.744 \pm 0.009	0.821 \pm 0.018	0.785 \pm 0.010
		0.918 \pm 0.010	0.837 \pm 0.012	0.843 \pm 0.011	0.831 \pm 0.013	5-6	1.971 \pm 0.088	0.625 \pm 0.044	0.785 \pm 0.009	0.866 \pm 0.022	0.820 \pm 0.009	0.878 \pm 0.014	0.844 \pm 0.017
		0.961 \pm 0.007	0.896 \pm 0.009	0.884 \pm 0.014	0.909 \pm 0.002	4	2.507 \pm 0.116	0.452 \pm 0.080	0.868 \pm 0.003	0.939 \pm 0.012	0.899 \pm 0.008	0.952 \pm 0.003	0.919 \pm 0.003

Table 16. Results for Scenario S5 using minutiae-based FOI saliency. Models trained using CYBORG in the large-data-availability context. Averaged over three runs.

Network	Alpha (α)	AUC	Accuracy	Bonafide Accuracy	Spoof Accuracy	Placement	d^*	FNR @ FPR = 1%	GLS20 ^U Accuracy	VBN ^U Accuracy	RFastPro ^U Accuracy	Wood Glue ^K Accuracy	Body Double ^K Accuracy
ResNet DenseNet Inception	0.9	0.989 \pm 0.001	0.915 \pm 0.002	0.996 \pm 0.002	0.829 \pm 0.004	3-4	3.222 \pm 0.049	0.134 \pm 0.009	0.750 \pm 0.012	0.900 \pm 0.001	0.782 \pm 0.006	0.909 \pm 0.007	0.885 \pm 0.006
		0.988 \pm 0.001	0.938 \pm 0.004	0.964 \pm 0.001	0.910 \pm 0.009	1-2	3.175 \pm 0.058	0.167 \pm 0.010	0.857 \pm 0.009	0.927 \pm 0.023	0.887 \pm 0.010	0.949 \pm 0.009	0.949 \pm 0.009
		0.990 \pm 0.002	0.916 \pm 0.010	0.993 \pm 0.001	0.832 \pm 0.021	3-4	3.308 \pm 0.093	0.144 \pm 0.012	0.745 \pm 0.027	0.915 \pm 0.011	0.786 \pm 0.041	0.928 \pm 0.024	0.875 \pm 0.010
ResNet DenseNet Inception	0.7	0.985 \pm 0.001	0.914 \pm 0.004	0.991 \pm 0.000	0.830 \pm 0.005	3-4	3.068 \pm 0.029	0.165 \pm 0.009	0.765 \pm 0.008	0.891 \pm 0.010	0.787 \pm 0.013	0.911 \pm 0.018	0.869 \pm 0.014
		0.972 \pm 0.005	0.912 \pm 0.009	0.917 \pm 0.012	0.907 \pm 0.006	3-4	2.708 \pm 0.112	0.333 \pm 0.031	0.850 \pm 0.011	0.942 \pm 0.006	0.881 \pm 0.009	0.973 \pm 0.002	0.940 \pm 0.002
		0.986 \pm 0.001	0.937 \pm 0.003	0.961 \pm 0.004	0.910 \pm 0.002	1-2	3.102 \pm 0.043	0.183 \pm 0.024	0.852 \pm 0.004	0.949 \pm 0.006	0.886 \pm 0.001	0.972 \pm 0.006	0.942 \pm 0.004
ResNet DenseNet Inception	0.5	0.951 \pm 0.013	0.877 \pm 0.014	0.944 \pm 0.019	0.804 \pm 0.009	4-5	2.355 \pm 0.182	0.329 \pm 0.036	0.747 \pm 0.011	0.848 \pm 0.016	0.776 \pm 0.006	0.857 \pm 0.013	0.847 \pm 0.004
		0.947 \pm 0.004	0.872 \pm 0.008	0.881 \pm 0.013	0.862 \pm 0.008	4-5	2.283 \pm 0.047	0.437 \pm 0.011	0.813 \pm 0.013	0.901 \pm 0.006	0.848 \pm 0.010	0.915 \pm 0.005	0.875 \pm 0.006
		0.981 \pm 0.003	0.924 \pm 0.005	0.935 \pm 0.013	0.912 \pm 0.019	3	2.934 \pm 0.085	0.234 \pm 0.022	0.854 \pm 0.027	0.966 \pm 0.014	0.880 \pm 0.023	0.973 \pm 0.011	0.946 \pm 0.013
ResNet DenseNet Inception	0.3	0.885 \pm 0.008	0.802 \pm 0.009	0.848 \pm 0.007	0.752 \pm 0.019	7	1.702 \pm 0.058	0.100 \pm 0.000	0.690 \pm 0.028	0.798 \pm 0.019	0.728 \pm 0.026	0.799 \pm 0.013	0.796 \pm 0.006
		0.919 \pm 0.006	0.836 \pm 0.007	0.836 \pm 0.005	0.835 \pm 0.008	5	1.978 \pm 0.051	0.567 \pm 0.025	0.793 \pm 0.011	0.869 \pm 0.007	0.827 \pm 0.011	0.879 \pm 0.005	0.840 \pm 0.008
		0.967 \pm 0.004	0.902 \pm 0.005	0.888 \pm 0.012	0.918 \pm 0.010	4	2.609 \pm 0.071	0.416 \pm 0.034	0.869 \pm 0.017	0.952 \pm 0.002	0.898 \pm 0.016	0.971 \pm 0.003	0.942 \pm 0.009
ResNet DenseNet Inception	0.1	0.842 \pm 0.005	0.760 \pm 0.005	0.784 \pm 0.013	0.734 \pm 0.005	10-11	1.416 \pm 0.032	1.000 \pm 0.000	0.679 \pm 0.002	0.768 \pm 0.004	0.711 \pm 0.002	0.789 \pm 0.016	0.769 \pm 0.020
		0.904 \pm 0.014	0.821 \pm 0.014	0.818 \pm 0.012	0.824 \pm 0.015	5-7	1.852 \pm 0.113	0.658 \pm 0.047	0.777 \pm 0.021	0.874 \pm 0.015	0.808 \pm 0.014	0.877 \pm 0.010	0.832 \pm 0.016
		0.948 \pm 0.009	0.878 \pm 0.012	0.861 \pm 0.007	0.896 \pm 0.017	4-5	2.302 \pm 0.126	0.561 \pm 0.066	0.855 \pm 0.022	0.940 \pm 0.010	0.880 \pm 0.016	0.942 \pm 0.008	0.902 \pm 0.021

Table 17. Results for Scenario S5 using minutiae-based AOI saliency. Models trained using CYBORG in the large-data-availability context. Averaged over three runs.

Network	Alpha (α)	AUC	Accuracy	Bonafide Accuracy	Spoof Accuracy	Placement	d^*	FNR @ FPR = 1%	GLS20 ^U Accuracy	VBN ^U Accuracy	RFastPro ^U Accuracy	Wood Glue ^K Accuracy	Body Double ^K Accuracy
ResNet DenseNet Inception	0.9	0.985 \pm 0.003	0.903 \pm 0.007	0.996 \pm 0.001	0.803 \pm 0.014	4	3.090 \pm 0.128	0.150 \pm 0.016	0.711 \pm 0.030	0.891 \pm 0.001	0.739 \pm 0.025	0.901 \pm 0.006	0.872 \pm 0.008
		0.930 \pm 0.026	0.847 \pm 0.020	0.938 \pm 0.033	0.769 \pm 0.007	5-6	2.123 \pm 0.274	0.415 \pm 0.022	0.632 \pm 0.003	0.919 \pm 0.015	0.684 \pm 0.004	0.909 \pm 0.017	0.846 \pm 0.021
		0.931 \pm 0.031	0.862 \pm 0.029	0.962 \pm 0.017	0.754 \pm 0.042	4-5	2.177 \pm 0.397	0.347 \pm 0.098	0.649 \pm 0.053	0.856 \pm 0.011	0.709 \pm 0.057	0.866 \pm 0.014	0.789 \pm 0.057
ResNet DenseNet Inception	0.7	0.982 \pm 0.002	0.907 \pm 0.004	0.990 \pm 0.000	0.817 \pm 0.008	4	2.979 \pm 0.079	0.183 \pm 0.008	0.732 \pm 0.015	0.879 \pm 0.011	0.774 \pm 0.017	0.891 \pm 0.004	0.885 \pm 0.008
		0.790 \pm 0.019	0.736 \pm 0.004	0.819 \pm 0.011	0.645 \pm 0.007	1							

Network	Alpha (α)	AUC	Accuracy	Bonafide Accuracy	Spoof Accuracy	Placement	d^*	FNR @ FPR = 1%	GLS20 ^U Accuracy	VBN ^U Accuracy	RFastPro ^U Accuracy	Wood Glue ^K Accuracy	Body Double ^K Accuracy
ResNet DenseNet Inception	0.9	0.983 \pm 0.003	0.895 \pm 0.005	0.994 \pm 0.001	0.788 \pm 0.011	4	2.995 \pm 0.101	0.170 \pm 0.008	0.709 \pm 0.019	0.885 \pm 0.003	0.727 \pm 0.016	0.887 \pm 0.009	0.826 \pm 0.008
		0.961 \pm 0.007	0.871 \pm 0.015	0.966 \pm 0.003	0.768 \pm 0.027	4-5	2.507 \pm 0.127	0.555 \pm 0.048	0.656 \pm 0.048	0.903 \pm 0.012	0.702 \pm 0.037	0.924 \pm 0.006	0.780 \pm 0.021
		0.991 \pm 0.002	0.906 \pm 0.011	0.996 \pm 0.001	0.808 \pm 0.023	3-4	3.328 \pm 0.090	0.138 \pm 0.012	0.710 \pm 0.031	0.922 \pm 0.006	0.734 \pm 0.038	0.933 \pm 0.003	0.859 \pm 0.027
ResNet DenseNet Inception	0.7	0.973 \pm 0.001	0.879 \pm 0.005	0.990 \pm 0.001	0.759 \pm 0.010	4-5	2.719 \pm 0.032	0.242 \pm 0.011	0.654 \pm 0.015	0.892 \pm 0.012	0.684 \pm 0.008	0.905 \pm 0.011	0.787 \pm 0.008
		0.940 \pm 0.004	0.842 \pm 0.006	0.950 \pm 0.004	0.727 \pm 0.015	5	2.201 \pm 0.052	0.723 \pm 0.030	0.610 \pm 0.024	0.881 \pm 0.011	0.651 \pm 0.015	0.905 \pm 0.006	0.729 \pm 0.015
		0.964 \pm 0.004	0.892 \pm 0.007	0.964 \pm 0.009	0.816 \pm 0.005	4	2.550 \pm 0.069	0.378 \pm 0.094	0.727 \pm 0.004	0.929 \pm 0.007	0.758 \pm 0.005	0.935 \pm 0.003	0.833 \pm 0.012
ResNet DenseNet Inception	0.5	0.948 \pm 0.003	0.840 \pm 0.006	0.975 \pm 0.003	0.694 \pm 0.013	5	2.306 \pm 0.039	0.522 \pm 0.023	0.579 \pm 0.015	0.835 \pm 0.010	0.622 \pm 0.017	0.865 \pm 0.004	0.706 \pm 0.018
		0.926 \pm 0.008	0.825 \pm 0.010	0.937 \pm 0.007	0.705 \pm 0.016	5-7	2.055 \pm 0.084	0.790 \pm 0.033	0.588 \pm 0.014	0.857 \pm 0.014	0.647 \pm 0.013	0.875 \pm 0.018	0.690 \pm 0.023
		0.940 \pm 0.024	0.857 \pm 0.028	0.935 \pm 0.023	0.774 \pm 0.033	4-6	2.239 \pm 0.267	0.597 \pm 0.127	0.673 \pm 0.040	0.906 \pm 0.022	0.710 \pm 0.036	0.922 \pm 0.014	0.776 \pm 0.045
ResNet DenseNet Inception	0.3	0.930 \pm 0.003	0.825 \pm 0.006	0.959 \pm 0.003	0.680 \pm 0.002	5	2.084 \pm 0.031	0.646 \pm 0.038	0.567 \pm 0.007	0.828 \pm 0.002	0.618 \pm 0.005	0.851 \pm 0.003	0.670 \pm 0.004
		0.909 \pm 0.010	0.813 \pm 0.006	0.926 \pm 0.012	0.692 \pm 0.001	6-7	1.888 \pm 0.081	0.807 \pm 0.011	0.578 \pm 0.004	0.845 \pm 0.007	0.629 \pm 0.008	0.873 \pm 0.006	0.672 \pm 0.009
		0.931 \pm 0.013	0.843 \pm 0.016	0.921 \pm 0.016	0.760 \pm 0.015	5-6	2.102 \pm 0.135	0.697 \pm 0.096	0.663 \pm 0.020	0.891 \pm 0.010	0.708 \pm 0.013	0.915 \pm 0.012	0.737 \pm 0.020
ResNet DenseNet Inception	0.1	0.930 \pm 0.001	0.820 \pm 0.002	0.949 \pm 0.003	0.681 \pm 0.008	6	2.085 \pm 0.014	0.666 \pm 0.008	0.572 \pm 0.013	0.829 \pm 0.004	0.621 \pm 0.014	0.846 \pm 0.004	0.664 \pm 0.006
		0.909 \pm 0.013	0.812 \pm 0.013	0.917 \pm 0.013	0.699 \pm 0.014	5-7	1.893 \pm 0.120	0.854 \pm 0.023	0.595 \pm 0.008	0.838 \pm 0.014	0.650 \pm 0.010	0.872 \pm 0.017	0.661 \pm 0.026
		0.924 \pm 0.005	0.831 \pm 0.008	0.908 \pm 0.003	0.748 \pm 0.015	5-6	2.030 \pm 0.048	0.774 \pm 0.015	0.646 \pm 0.020	0.881 \pm 0.013	0.691 \pm 0.015	0.907 \pm 0.007	0.733 \pm 0.020

Table 19. **Results for Scenario S5 using low-quality map saliency.** Models trained using CYBORG in the large-data-availability context. Averaged over three runs.